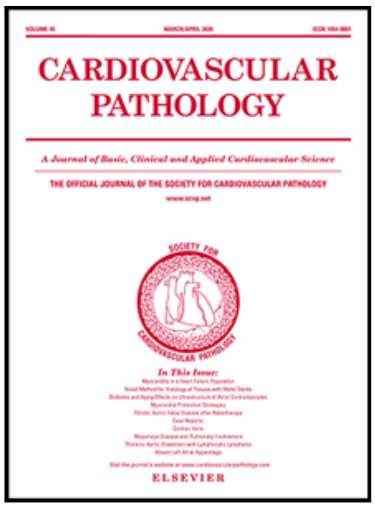

Ultrastructural Cardiac Pathology: The Wide (yet so very small) World of Cardiac Electron Microscopy

Gregory A. Fishbein , Melanie C. Bois , Giulia d'Amati , Carolyn Glass , Laura Masuelli , E. Rene Rodriguez , Michael A. Seidman

PII: S1054-8807(24)00066-8
DOI: https://doi.org/10.1016/j.carpath.2024.107670
Reference: CVP 107670

To appear in: *Cardiovascular Pathology*

Received date: 9 March 2024
Revised date: 7 June 2024
Accepted date: 9 June 2024

Please cite this article as: Gregory A. Fishbein , Melanie C. Bois , Giulia d'Amati , Carolyn Glass , Laura Masuelli , E. Rene Rodriguez , Michael A. Seidman , Ultrastructural Cardiac Pathology: The Wide (yet so very small) World of Cardiac Electron Microscopy, *Cardiovascular Pathology* (2024), doi: https://doi.org/10.1016/j.carpath.2024.107670

Highlights

- Electron microscopy (EM) interpretation is a lost art, even in academic centers.
- There remain situations in which EM is the best or only ancillary test to ascertain a specific diagnosis.
- This article reviews EM as it pertains to myocardial tissue and provides illustrative examples of the spectrum of ultrastructural cardiac pathology seen in storage/metabolic diseases, cardiomyopathies, infiltrative disorders, and cardiotoxicities.

Ultrastructural Cardiac Pathology: The Wide (yet so very small) World of Cardiac Electron Microscopy

Gregory A. Fishbein[1], Melanie C. Bois[2], Giulia d'Amati[3], Carolyn Glass[4], Laura Masuelli[3], E. Rene Rodriguez[5], Michael A. Seidman[6]

1. University of California, Los Angeles, David Geffen School of Medicine, Los Angeles, CA, USA

2. Mayo Clinic, Rochester, MN, USA

3. Sapienza, University of Rome, Rome, Italy

4. Duke University, Durham, NC, USA

5. Cleveland Clinic, Cleveland, OH, USA

6. University Health Network, Toronto, Canada

Corresponding author: Gregory A. Fishbein, gfishbein@mednet.ucla.edu

Department of Pathology & Lab Medicine

10833 Le Conte Ave, CHS 27-061 C4

Los Angeles, CA 90095

Abstract

Electron microscopy (EM) was a popular diagnostic tool in the 1970s and early 80s. With the adoption of newer, less expensive techniques, such as immunohistochemistry, the role of EM in diagnostic surgical pathology has dwindled substantially. Nowadays, even in academic centers, EM interpretation is relegated to renal pathologists and the handful of (aging) pathologists with experience using the technique. As such, EM interpretation is truly arcane—understood by few and mysterious to many. Nevertheless, there remain situations in which EM is the best or only ancillary test to ascertain a specific diagnosis. Thus, there remains a critical need for the younger generation of surgical pathologists to learn EM interpretation. Recognizing this need, cardiac EM was made the theme of the Cardiovascular Evening Specialty Conference at the 2023 United States and Canadian Academy of Pathology (USCAP) annual meeting in New Orleans, Louisiana. Each of the speakers contributed their part to this article, the purpose of which is to review EM as it pertains to myocardial tissue and provide illustrative examples of the spectrum of ultrastructural cardiac pathology seen in storage/metabolic diseases, cardiomyopathies, infiltrative disorders, and cardiotoxicities.

Keywords: electron microscopy, cardiac pathology, cardiomyopathy, infiltrative disorders, cardiotoxicity, storage diseases

Abbreviations: EM - electron microscopy; TEM – transmission electron microscopy; ACM – arrhythmogenic cardiomyopathy; HCM – hypertrophic cardiomyopathy; LCDD – light chain deposition disease

Funding: This research did not receive any specific grant from funding agencies in the public, commercial, or not-for-profit sectors.

1. Introduction

Electron microscopy (EM) was a popular diagnostic tool in the 1970s and early 80s. With the adoption of newer, less expensive techniques, such as immunohistochemistry, the role of EM in diagnostic surgical pathology has dwindled substantially. Nowadays, even in academic centers, EM interpretation is relegated to renal pathologists and the handful of (aging) pathologists with experience using the technique. As such, EM interpretation is truly arcane—understood by few and mysterious to many. Nevertheless, there remain situations in which EM is the best or only ancillary test to ascertain a specific diagnosis. Thus, there remains a critical need for the younger generation of surgical pathologists to learn EM interpretation. Recognizing this need, cardiac EM was made the theme of the Cardiovascular Evening Specialty Conference at the 2023 United States and Canadian Academy of Pathology (USCAP) annual meeting in New Orleans, Louisiana. Each of the speakers contributed their part to this article, the purpose of which is to review EM as it pertains to myocardial tissue and provide illustrative examples of the spectrum of ultrastructural cardiac pathology seen in storage/metabolic diseases, cardiomyopathies, infiltrative disorders, and cardiotoxicities.

1.1. Basics of electron microscopy

EM has been developed to increase the resolution of optical microscopy. It uses electronic wavelengths about five orders of magnitude lower than the lowest wavelength of visible light. The two primary techniques are transmission and scanning EM. Both use beams of electrons, generated by heating a tungsten filament or a FEG (Field Emission Gun), focused by electromagnetic lenses, and accelerated through an electrical potential in a high vacuum to avoid electron scattering by air molecules. In transmission electron microscopy (TEM) the electronic beam is transmitted through ultrathin sections allowing the inspection of the sub-cellular details. The electrons are then projected onto a fluorescent screen, and the final image is the result of differences in the electronic density of the trans-illuminated sample. The image

can be magnified up to one million folds by specific lenses. In scanning electron microscopy (SEM) the electronic beam scans the specimen surface to generate three-dimensional ultrastructural images [1].

In cardiovascular pathology, transmission electron microscopy can be a useful diagnostic tool in specific settings. The light microscopic findings of unexplained myocyte vacuolization or peculiar cytoplasmic inclusions may require ultrastructural examination by EM for definitive characterization. Clinical suspicion of infiltrative and metabolic disorders may also prompt ultrastructural analysis.

Specific technical requirements are necessary to achieve good-quality images, starting with tissue preservation. The optimal fixative is glutaraldehyde (2.5% in phosphate buffer). To avoid deterioration of subcellular structures, tissue samples must be extremely small (up to 1 mm^3) to obtain a rapid fixative penetration. Moreover, post-fixation in osmium tetroxide (OsO_4) is required to preserve membrane lipids. Another important technical issue is the thickness of sections. Since the electron beam cannot penetrate specimens thicker than 80-100 nm, biological samples must be embedded into hard plastic resins and sectioned with an ultramicrotome using glass or diamond blades to obtain ultrathin sections (40-90 nm thick). Sections are placed on metallic grids and stained with a combination of uranyl acetate and lead citrate, both containing heavy metals, to enhance the contrast between the intracellular structures [2].

It should be noted that diagnostic electron microscopy may still be performed under suboptimal conditions. If fresh tissue is not available, wet formalin-fixed tissue may be post-fixed in glutaraldehyde and submitted for routine processing as described above. Autopsy and calcified [3] tissues may also be used. Tissue can even be carved out of paraffin blocks [4]. The resulting images may exhibit deformed normal structures and preservation artifacts [5]; however,

particularly in the setting of infiltrative disorders (e.g. amyloidosis) and inborn errors of metabolism, abundant diagnostic material may still be present and readily recognizable.

1.2. Normal cardiac ultrastructure

1.2.1. Cardiac myocytes: the contractile and junctional apparatus

Normal ventricular cardiomyocytes (Fig. 1a) measure approximately 100 μm in length, with a centrally located nucleus. In the adult myocardium up to 10% of myocytes have more than one nucleus. The sarcoplasm is packed with well-organized sarcomeres (Fig. 1b), which are the functional units of cardiac myocytes. They are linked in series at the Z-lines and arranged in parallel to form the myofibrils. Each sarcomere consists of a hexagonal network of thin, actin-containing, and thick myosin-containing filaments, between two Z-lines (Fig. 1c). Actin filaments are anchored to the Z-lines, while myosin filaments are interconnected in the middle of the sarcomere at the M-band. Sliding of thin over thick filaments results in contraction, with sarcomere shortening. Contraction is regulated by tropomyosins, running over the surface of actin filaments. The giant protein titin extends from the Z-line to the M-band, stabilizing contraction and favoring the elastic recoil of the sarcomere [6]. Cardiac myocytes are electrically and mechanically linked to each other by a complex junctional system, the intercalated disc (Fig. 1d). The intercalated disc joins end-to-end cardiac myocytes and has a transverse and a longitudinal portion. Within the intercalated discs there are specialized intercellular junctions, responsible for the electrical and mechanical coupling of myocytes. The fascia adherens anchors actin filaments to the sarcolemma, and the desmosome is the site of sarcolemmal anchoring for the cytoskeletal intermediate filaments desmin and vimentin. Both provide adhesion between adjacent myocytes. The gap junctions are in the longitudinal portion of the intercalated disc. They mediate action potential propagation between cells, to synchronize cardiac contraction [7–9].

1.2.2. Other intracellular components and organelles

Human cardiomyocytes generally contain one or two nuclei. The nuclei are oval-shaped, located centrally, mostly composed of euchromatin with scarce heterochromatin arranged in the periphery or dispersed in small clumps. One or two electron-dense nucleoli are usually clearly visible within the nucleus [10]. Chromatin-bare regions of the nuclear membrane may exhibit uniformly spaced nuclear pores measuring 500 Å in diameter, sometimes with a central granule. The sarcoplasm contains desmin and vimentin intermediate filaments and a network of membranes surrounding the myofilaments, the sarcoplasmic reticulum. It is the site of storage and transport of calcium, the release of which is required to initiate muscle contraction. It contacts the sarcolemma and its invaginations, the T-tubule system. The T tubules (Fig. 1b) spread the electrical impulse through the myofibers, and the sarcoplasmic reticulum mediates the excitation-contraction coupling by releasing calcium. Cardiac myocytes also contain numerous organelles, especially mitochondria. Ventricular myocytes contain much more mitochondria than skeletal muscle (~35% vs 3-8% of cell volume) reflecting the extreme dependence of cardiac muscle on aerobic metabolism [11]. They are commonly seen close to gap junctions, contractile elements, and sarcoplasmic reticulum (Fig. 1d). Glycogen granules and fat droplets are also present, the latter in close proximity with mitochondria, representing a source of energy through fatty acid oxidation. Cardiac myocytes also contain a Golgi apparatus and a few lysosomes, normally in the perinuclear region. As other post-mitotic cells, with aging cardiac myocytes accumulate lipofuscin within lysosomes. Lipofuscin is made from highly oxidized proteins and lipids that cannot be digested in the ubiquitin-proteasome system and accumulate in lysosomes. Lipofuscin appears as electron-dense, membrane-bound granules, heterogenous in size and in structure with associated lipidic components. It is often located in the perinuclear region [12].

1.2.3. Differences between atrial and ventricular cardiomyocytes

Atrial cardiomyocytes are usually elliptical in shape with a centrally located nucleus. They are approximately 20-30 µm long. The cytoplasm is packed with working sarcomeres, indistinguishable from the ventricular ones. Characteristically, the transverse tubular system is less developed than in ventricular cardiomyocytes, with a decrease in the surface membrane. Elongated mitochondria are located between myofibrils. Moreover, dense secretory granules (Fig. 2), mainly responsible for the secretion of atrial natriuretic peptide (ANP), also called atrial natriuretic factor (ANF), are visible in the sarcoplasm in the perinuclear areas and close to the Golgi apparatus. Less developed intercalated discs connect end-to-end consecutive cardiomyocytes; atrial cardiomyocytes also display lateral linear intercellular junctions, mainly represented by desmosomes [13].

1.2.4. Purkinje cells

Purkinje cells (Fig. 3) are specialized rapidly conducting extranodal cardiomyocytes. At 70-80 µm in diameter, they are normally the widest cells in the heart [13]. Within the cytoplasm are linearly arranged sarcomeres, mitochondria, and abundant pools of glycogen. Notably, the T-tubule system is absent. Purkinje cells form discrete bands of the conduction system in the subendocardial left and right ventricles. They are also found in the atria, but do not form morphologically discrete tracts throughout the atrial tissue.

1.2.5. The cardiac interstitium

Both atrial and ventricular cardiomyocytes are surrounded and connected to the interstitium by a well-organized basal membrane (Fig. 1b) composed by type IV collagen, laminin, proteoglycans, and glycoproteins [14]. The cardiac interstitium is a three-dimensional dynamic network located among cardiomyocytes, comprising banded collagen fibers (type I and III collagens) (Fig. 1a), proteoglycans, non-collagenous glycoproteins, and extracellular proteases. The extracellular matrix is synthesized by cardiac fibroblasts, and it is necessary to maintain the shape, thickness, and alignment of cardiomyocytes during heart contraction, improving their

resistance to deformation. The cellular component of the interstitium also comprises endothelial cells, smooth muscle cells, pericytes, and nervous cells (Fig. 1, e-f). Myocardial interstitial remodeling plays an important role in heart pathophysiology since acquired or congenital defects of the extracellular matrix can contribute to the onset of abnormalities in myocardial architecture and or functions.

1.3. Principles of cardiac EM interpretation

1.3.1. Specimen preparation and microscopic technique

Ultrastructural examination of the heart should ideally be systematic and reproducible. Planning ahead how to procure and process the tissue to be examined is key. Such planning includes:

1. Ensure proper fixation of the specimen, which requires small pieces of tissue (1 mm^3), and fixation in an aldehyde. There are several possibilities to fix the specimen. For practical purposes a mixture of formaldehyde and glutaraldehyde should be available in any pathology department. The fast penetration of formaldehyde followed by the glutaraldehyde produces excellent fixation of proteins and nucleic acids for transmission electron microscopy [15].

2. Whenever possible, pay attention to the orientation of the muscle bundles/fibers in the specimen. Choose longitudinal bundles of myocardial fibers and keep the orientation of these as you select the sample that will go for electron microscopy. Ascertain that when embedding the tissue in your polymer/resin of choice, the myocyte bundles are preferably oriented in a longitudinal manner. This can provide easier identification of structure and organelles and accurate measurements. These steps are best performed using a dissection microscope. If a technician will be performing these steps, a discussion regarding the optimal orientation of tissue is prudent.

3. Remember that formalin-fixed tissue is still useful for electron microscopy, if post-fixed in glutaraldehyde. In addition, formalin-fixed wet tissue can be stained for lipid substances which may correlate with ultrastructural features such as lipid moieties.

4. The selection of the target areas for electron microscopy is easily done in the “semi-thin” 1-micron thick plastic embedded tissue sections stained with toluidine blue. In current practice, the glass slides may be scanned, and the target areas marked in the electronic image files. Longitudinally oriented myocytes are ideal to assess the sarcoplasmic structures, membrane components, basal laminae, interstitial components, and capillaries.

5. Examination of the ultrathin grids should be performed at several magnifications. Five to 6 images at low magnification (X3000 – 4000) should be performed to assess the orientation of the cells on the grid and correlate with the chosen fields on toluidine blue. Also, it can show areas of contraction band artifact or too many myocytes in oblique or cross sections. Six to 8 images at X8000 - X12000 can provide enough detail to assess most cellular components as described below. Six to 8 additional images can be taken at X18000 to X22000. If the images are acquired by a technician, communicate to them the potential diagnostic findings based on the clinical and/or light microscopic differential diagnosis. Providing photographic examples of what to look for can be very helpful.

1.3.2. Examination of the sarcoplasmic elements and myocyte membranes

1. Sarcomeres.

Before the advent of electron microscopy, examination of striated muscle under polarized light revealed two bands producing the striations. One is anisotropic (A-band) and the other is isotropic (I-band), which measures 0.7 µm in length. The A-band is the wide central electron dense band in the center of the sarcomere (Fig. 3), measuring 1.5 µm in length. It is bisected by the M-band (Mittelinie = Middle line). The M-band shows 5 fine divisions (M-lines) of alternating

electron dense and electron lucent material which correspond to the myomesin complexes that organize the anchoring of the thick filaments. The L-line (also called pseudo-H or Helle = light or clear) is present at each side of the M-band. In this area there are no cross bridges between the thick filaments and there are no overlapping thin filaments. The sarcomere is delimited by the two electron dense Z-discs or bands (Zwischenscheibe = middle or dividing disc). The Z-band bisects the I-band. The N-Line (Nebenscheibe = neighboring disc) bisects each half of the I-band.

2. Mitochondria and sarcoplasmic reticulum.

Mitochondria are present between the myofibrils and are aligned between the Z-bands. One to two mitochondria per sarcomere is normal. The sarcoplasmic reticulum is commonly seen in cross sections at the level of the Z-bands. The T-tubules in ventricular myocytes are also present at the level of Z-bands forming diads or triads with the sarcoplasmic reticulum. The T-tubular system is further described with the sarcolemma (Fig. 3).

3. Lysosomes, lipid vacuoles and other organelles.

Lysosomes are double membrane bound roughly round vesicles measuring with slightly electron dense material (Fig. 4). They measure on average 300-580 nm. Occasional lipid filled vacuoles are considered normal. Abundant larger lipid vacuoles are abnormal. These structures are difficult to differentiate from lysosomes as they are also double membrane bound and show slightly increased electron density (Fig. 5). When abundant they can also be variable in size. The lipid vacuoles tend to be metachromatic in toluidine blue-stained plastic embedded sections.

3. Other membranous structures within myocytes.

Both rough endoplasmic reticulum and the Golgi apparatus are present in cardiac myocytes but they are difficult to identify in ultrastructural examination (Fig. 6).

4. Sarcolemma, pinocytic vesicles and T-tubules.

The sarcolemma of myocytes is the cell membrane of the myocytes. It has different functional domains. On electron microscopy it is electron dense and measure about 4 nm in thickness. It is surrounded by normal basal lamina, and it is common to observe pinocytic vesicles along the sarcolemma or opening into the extracellular space (Fig. 7). The basal lamina of the myocytes is slightly less electron dense and measures 20-50 nm thick. The sarcolemma invaginates into the myocytes perpendicular to their longitudinal axis thus forming transverse tubular structures (T-tubules) which are in direct contact with the extracellular environment and thus facilitate exchange of oxygen, ions, or any solutes present in the extracellular environment. These tubules penetrate into the core of the myocytes, they maintain their location in register with the Z-bands where they are joined by the sarcoplasmic reticulum forming the diads and triads.

5. Intercalated discs.

The intercalated discs (Fig. 8) are specialized components of the myocyte membrane system which provide structural (desmosomes), mechanical (adherens junctions) and electrical (nexuses or gap junctions) connections between cells. The intercalated discs are present in the end-to-end as well as side-to-side portions of the sarcolemma in fetuses and infants. Soon after birth the intercalated discs in ventricular myocytes are almost exclusively present at the ends of the longitudinal axes of the myocytes.

The cell structure and organelles vary in atrial, ventricular, and Purkinje myocytes as shown in Table 1. Various structures and their typical measurements are shown in Table 2.

2. Ultrastructural cardiac pathology

2.1. Inborn errors of metabolism

TEM examination is a useful tool to evaluate alterations of different compartments of the cardiac myocytes that may be secondary to storage of diverse metabolic substrates. Ordinary light microscopy may only show vacuolated myocytes. It is the role of TEM to reveal what is inside the vacuoles. The ultrastructural evaluation may show small or large lysosomes with granular or electron dense homogeneous contents; granules in the sarcoplasm, predominantly perinuclear accumulation of organelles (mitochondria, secondary lysosomes), inclusions or clearance of that space; pigmented granules, lamellar myelin-like structures, sarcoplasmic inclusions or deposition of proteins or intermediate filaments. The main categories are in Table 3. In this section, some selected examples of ultrastructural pathology of metabolic diseases will be presented.

2.1.1. Disorders of glycogen metabolism

The cardiac myocytes contain glycogen in several compartments, including lysosomes, free glycogen in the sarcoplasmic reticulum and in mitochondria. When there is excess glycogen in the myocytes, it is commonly seen in the sarcoplasm. Sarcoplasmic glycogen may be present throughout the myocytes in glycogen storage diseases such as glycogen storage disease IV (Andersen's disease) and PRKAG2 deficiency (Fig. 9a) [16]. Notably, similar accumulation can be seen patient who have mutations in sarcomeric proteins, such as myosin binding protein C3 (MyBPC3). Intralysosomal glycogen storage is defined as glycogen contained within lysosomes. Ultrastructurally, the identification of membrane-bound glycogen requires the presence of distinct double membranes to identify the lysosomes. Intralysosomal glycogen (Fig. 9b) may be seen in patients with glycogen storage disease II (Pompe disease) and *LAMP2* mutations (Danon disease) [17].

2.1.2. Lysosomal storage diseases

In addition to Intralysosomal glycogen storage, the cardiac myocytes can also exhibit pathologic storage of fatty acids in the form of microvesicular steatosis (Fig. 9c). This may be genetic or acquired or even induced by viral infections.

2.1.3. Fabry's disease

Fabry's disease is an X-linked disease caused by a deficiency of α-galactosidase A activity. It is a systemic disease that results in accumulation of glycosphingolipids (ceramide trihexoside). This accumulation is manifested by formation of lamellar structure that resemble myelin. Ultrastructurally myelin-like figures (Fig. 9d) are not specific for Fabry's disease but when abundant and consistent with the cardiac or systemic phenotype, they can be diagnostic of Fabry's disease.

2.1.4. Mitochondrial disorders

Mitochondrial disorders can show marked proliferation of mitochondria within the cardiac myocytes (Fig. 10.) Pleomorphism (a.k.a. pleoconia) of mitochondria ranging from very small to very large (a.k.a. megaconia) or bizarre shaped mitochondria can be present. Alterations of the mitochondrial cristae are important to recognize. These alterations go from the parallel arrays that are perpendicular to the long axis of a mitochondrion to circular arrangement of the cristae which resembles a fingerprint to large annular formations. Proliferation of mitochondria can be due to mutation in the mitochondrial genome encoded proteins or due to Mendelian gene mutations.

2.2. Cardiomyopathy

In the current era, most cardiomyopathy is diagnosed clinically and/or with the help of genetic testing. EM may nevertheless demonstrate characteristic findings, even in tissue specimens lacking diagnostic pathologic findings by light microscopy. Such specimens may include native endomyocardial biopsies, left ventricular assist device apical core excisions, explants and

autopsy hearts. Ultrastructural pathology may be identified by EM in a number of cardiomyopathies, including but not limited to arrhythmogenic cardiomyopathy (ACM), desmin-related myofibrillar myopathy (DRM) involving cardiac muscle, hypertrophic cardiomyopathy (HCM) and lamin A/C cardiomyopathy (LMNA).

2.2.1. Arrhythmogenic cardiomyopathy (ACM)

ACM, also called arrhythmogenic right ventricular cardiomyopathy (ARVC) and formerly arrhythmogenic right ventricular dysplasia (ARVD), predominantly affects the right ventricle, sometimes with left ventricular involvement, and is characterized by myocardial atrophy that progresses to fibro-fatty replacement. ACM is familial in up to 50% of cases and can be associated with life-threatening ventricular arrhythmias and sudden death. Gene alterations in proteins critical for intercellular junctions, mechanical coupling of cardiomyocytes and continuous cell-to-cell connection to sarcomeric actin and intermediate filaments are affected. These genes include desmoglein-2, desmoplakin, plakoglobin and plakophilin-2 which encode desmosomal proteins that provide links between cells, connect intermediate filaments of adjacent cells and provide structural integrity of the cellular cytoskeleton [18].

Kaplan et al. [19] reported widening of intercalated disc intercellular distance as well as misalignment of hemidesmosomes (Fig. 11). Fujita et al. [20] described numerous lipid droplets of varying sizes were observed within the cardiomyocytes, some which were extremely large. Additional findings included several altered nuclei present in the periphery of the cardiomyocytes, reticular formation of nuclear chromatin within nuclei, disruptions of the plasma membrane and dissociation of intercellular junctions. Myofibrillar lysis and increased glycogen granules and lipofuscin in cardiomyocytes were also associated non-specific findings. Basso et al. systematically investigated the ultrastructural evidence of intercalated disc remodelling in ACM in endomyocardial biopsies with residual myocardium of 59% [21]. Myocyte intercalated discs in ACM, idiopathic dilated cardiomyopathy and controls were examined by EM.

Pathogenic gene mutations were identified in 48% and included desmoglein-2, desmoplakin and plakophilin-2. Abnormal small junctions were observed in 52% of ACM cases and abnormally located Ds were identified in 75%.

2.2.2. Desmin-related myofibrillar myopathy (DRM)

Genetic mutations involving desmin, an important subunit of the intermediate filament in cardiac, skeletal and smooth muscles, may also occur. Desmin-related myofibrillar myopathy (DRM) is a cardiac and skeletal muscle disease caused by more than 40 different desmin mutations resulting in skeletal muscle disease preceding cardiac involvement. In cases involving the cardiac muscle, the most common phenotype is dilated cardiomyopathy (DCM), followed by restrictive cardiomyopathy, ACM [22] and HCM. A rare variant p.(Q364H) associated with decreased myocardial expression of desmin and absent desmin aggregates has been associated with familial left ventricular non-compaction cardiomyopathy. Desmin filaments play a critical role in the maintenance of structural integrity in mechanically stressed tissues. Cardiac biopsies have shown cytoplasmic aggregations of intermediate filaments and a secondary mitochondrial dysfunction in desminopathy. The characteristic ultrastructural feature of DRM is the formation of amorphous filamentous material and inclusions in cardiomyocyte cytoplasm consistent with desmin aggregates [23] (Fig. 12). Clusters of increased mitochondria with an aberrant distribution have also been described [24].

2.2.3. Hypertrophic cardiomyopathy (HCM)

HCM is an inherited cardiomyopathy, most commonly due to mutations in sarcomere protein encoding genes *MYH7*, *MYBPC3*, *TNNT2*, and *TNNI3*. Cardiac dysfunction results from a chronic increase in cardiac workload, ATP utilization and perturbations in oxidative mitochondrial metabolism [25]. Frequently hypertrophy of the left ventricle is asymmetric favoring the interventricular septum, resulting in left ventricular outflow tract obstruction.

Myocardial disarray was first described as a prominent microscopic feature of HCM by Teare in his initial report of the cardiac anatomic findings. Thickened intramural coronary arteries with fibromuscular proliferation and interstitial fibrosis are other findings observed by light microscopy. Myocyte disarray involving bundles of myocytes and individual myocytes have been evaluated using EM, showing myofibrils coursing in different directions (Fig 12). Large sarcoplasmic deposits of glycogen may be present, mimicking glycogen storage disease .

Nollet et al. studied interventricular septal tissue of 59 consecutive patients status post myectomy, 47 of whom underwent genetic testing with causative mutations identified in 23 patients [26]. EM studies in 19 patients showed mitochondrial abnormalities. Although an abundance of myofibrils and mitochondria, or changes in cristae swelling were observed in severe HCM, there was severe disruption of mitochondrial organization relative to myofibrils, compared to the control cohort. The average mitochondrial size was also significantly lower in HCM patients, suggesting evidence of mitochondrial fragmentation. Studies by Ranjbarvaziri et al. further support HCM is associated with energetic stress, metabolic signaling and mitochondrial dysfunction [27]. EM showed marked disruption in mitochondrial ultrastructure with swollen interfibrillar mitochondria with disorganized and reduced cristae density. Quantification of cristae density revealed a significant percent increase in severely damaged cristae and disruption of cristae architecture, with a trend towards a decrease in mitochondrial size.

2.2.4. Lamin A/C (LMNA) cardiomyopathy

Finally, lamin A/C cardiomyopathy is another cardiomyopathy with unique ultrastructural features that may be identified by EM. Lamin A/C cardiomyopathy is a young onset, familial dilated cardiomyopathy which commonly requires heart transplantation. Lamins A and C are major components of the nuclear lamina, the meshwork associated with the inner nuclear membrane. Greater than 45 mutations in the lamin A/C (*LMNA*) gene have been identified and

result in a phenotype of DCM with conduction system disease or other myopathies such as limb girdle muscular dystrophy, Emery-Dreifuss muscular dystrophy and lipodystrophy. The lamin A/C genotype-positive subjects studied by Hasselberg et al. had a high frequency of atrioventricular block, atrial fibrillation, ventricular arrythmias and reduced left ventricular function. Cardiac magnetic resonance imaging showed late gadolinium enhancement representative of fibrosis in the basal and mid-interventricular septum in 46% of subjects [28]. In one of the earliest *LMNA* studies that included pathologic tissue, Arbustini et al. showed non-specific myocyte damage and interstitial fibrosis by light microscopy [29]. However, EM revealed more specific features including focal nuclear membrane disruptions, bleb formation and nuclear pore clustering in cardiomyocytes, compatible with ultrastructural evidence of delamination. In a familial cardiomyopathy case with early-onset cardiac fibrosis due to a *LMNA* deletion, Direcks et al. described detailed morphologic changes in nuclear architecture by EM [30]. Most profoundly, the nuclear shape was very irregular with extensive convolution, along with disruption of the nuclear lamina (Fig. 14).

2.2.5 TTN-associated dilated cardiomyopathy.

Herman et al. [31] described irregular nuclear membranes evident on brightfield microscopy in cases of dilated cardiomyopathy due to *TTN* truncation mutations. The same cases also showed dramatic ultrastructural changes to the nuclear membranes [personal communication] (Fig. 15). At this time, of note, the sensitivity and specificity of nuclear contour irregularity is uncertain and warrants further study.

2.3 Infiltrative disorders

2.3.1. Amyloidosis

Amyloidosis is a general term used to describe a family of diseases characterized by the deposition of amyloid fibrils in tissues. Erroneously named based on the Latin word for starch,

amyloid is a protein [32]. There are over 30 human proteins that form amyloid; at the time of this publication, 12 have been described to involve the heart (Table 4) [32,33].The most common systemic amyloidoses affecting the heart include transthyretin amyloidosis (ATTR), light chain amyloidosis (AL), and amyloid A amyloidosis (AA). Of note, atrial natriuretic factor may form amyloid deposits (AANF); however, deposition is localized to the heart and does not manifest as systemic disease.

Grossly, affected hearts are firm and appear rubbery. Waxy deposits may be seen on the endocardial surfaces and valves. Microscopically, amyloid appears as amorphous eosinophilic material filling the interstitial spaces (Fig. 16). The material may surround individual myocytes or aggregate, forming discrete nodules. Endocardial, vascular, and epicardial involvement may be seen. Characteristically, amyloid proteins bind the dye Congo red and exhibit yellow to “apple” green birefringence under polarized light. In addition to Congo red, stains used to confirm the presence of amyloid include crystal violet, sulfated Alcian blue (SAB), and thioflavin S or T. Amyloid also has a distinctive amphophilic, gray-blue hue on Masson trichrome stain. Using these histochemical stains, the diagnosis of cardiac amyloidosis can usually be made by light microscopy alone. However, TEM may be helpful when the burden of amyloid is low, or the light microscopic morphology is questionable.

On TEM, amyloid deposits are mainly composed of extracellular bundles of non-branching fibrils ranging from 6-13 nm in diameter and 100-1600 nm in length (Fig. 16c,d) [34]. The fibrils are most frequently straight but may occasionally be curved. They are haphazardly arranged and often overlapping, in contrast to collagen fibrils, which are organized and separated from each other by a small amount of space. Collagen fibrils can also be distinguished from amyloid by their larger size, 20-500 nm in diameter [35], and characteristic banding pattern. Although the morphology of the amyloid fibrils varies slightly depending on the amyloid subtype, it is not possible to determine the amyloid protein based on ultrastructural morphology alone. Amyloid

subtyping can, however, be performed using immuno-electron microscopy, in which binding of gold-labeled amyloid type-specific antibodies to the corresponding amyloid fibrils is visualized by the agglomeration of gold colloid particles within the amyloid deposits.

2.3.2. Light Chain Deposition Disease

Like AL, light chain deposition disease (LCDD) results when monoclonal light chains (usually kappa) deposit around cardiomyocytes and other cells. Cardiac involvement in LCDD is rare. It is seen in the setting of plasma cell dyscrasias, typically multiple myeloma, and closely mimics amyloidosis in that setting [36]. Morphologically similar to amyloid by light microscopy, LCDD manifests as amorphous eosinophilic material on H&E, often within the walls of blood vessels. However, in the heart the deposits may be inconspicuous. Unlike AL, in which the misfolded light chains form amyloid fibrils, the deposits of LCDD do not stain with Congo red, crystal violet, or thioflavin T [37]. Unlike amyloid, which stains gray-blue with Masson trichrome (MT) and seafoam green with SAB, the deposits of LCDD appear crimson red and salmon pink when stained with MT and SAB, respectively [38]. The deposits are PAS-positive and diastase-resistant.

Ultrastructurally, the electron-dense deposits in LCDD do not resemble amyloid. They are granular, rather than fibrillary, and have been described as “powdery” [39] or like cotton balls [40] (Fig. 17). They accumulate on the sarcoplasmic membrane of the cardiomyocytes, around interstitial cells, and within blood vessels. Since the deposits may not be apparent on H&E and do not stain with Congo red, TEM should be performed in all cases in which AL is suspected but the EMB is negative for amyloid.

2.3.3. Iron Overload

“…the iron heart is not a strong heart but a weak one” [41]. Normally, there is no stainable iron in the heart. Thus, the light microscopic finding of iron in cardiomyocytes is definitively

pathologic. Cardiac iron deposits (CID) may be seen in the setting of transfusion dependent anemias or hereditary hemochromatosis. While heart failure is a leading cause of death in patients with transfusion dependent anemias, it is rarely a direct cause of death in patients with hereditary hemochromatosis [42,43]. The failing heart in these settings may have either a dilated or restrictive phenotype. Affected hearts may appear rusty brown. Microscopically, H&E-stained sections show granular brown deposits within cardiomyocytes and occasional interstitial cells. The deposits may easily be mistaken for lipofuscin; histochemical staining for iron is used to confirm/exclude the diagnosis.

CID can be easily demonstrated microscopically using Prussian blue histochemistry; iron may even be visible grossly. Therefore, the use of TEM in the setting of iron overload is largely academic. Ultrastructurally, CID consist of aggregates of electron dense particles measuring roughly 6 nm in diameter, and may be seen within cardiomyocytes and interstitial cells, regardless of the etiology (Fig. 18). [41] In cardiomyocytes, CID tend to deposit in paranuclear—small aggregates adjacent to the nucleus, perinuclear—more extensive deposition surrounding the nucleus, and/or diffuse cytoplasmic patterns [44]. CID may also be seen in the cardiomyocyte nucleus and mitochondria. The deposition is most extensive in the outer third of the ventricular myocardium, and more extensive in the ventricles than the atria and conduction system [41,44]

2.3.4. Viral Myocarditis

Due to their small size, most viruses can only be seen by TEM. While TEM remains an essential tool to elucidate new viruses, the clinical utility of TEM to diagnose viral infection has declined with the adoption of more sensitive techniques such as enzyme-linked immunosorbent assay (ELISA), polymerase chain reaction (PCR), immunohistochemistry (IHC), and in situ hybridization (ish). Viral infection of the heart manifests as disseminated focal lesions [45]. Since the field of view of TEM is small and restricted, localization of virally infected cells is a

technical challenge, and is best guided by light microscopy if inclusion bodies are identifiable. Otherwise, using TEM to identify viral particles in a biopsy is like looking for a needle in a haystack.

Nonetheless, successful EM can localize the virion to the infected cell type (e.g. endothelium vs. myocardium vs. etc.), and can contribute to understanding the infectious agent itself, the value of which became evident during the recent COVID-19 pandemic [46,47]. This said, confirming that the particles are indeed virus derived requires high resolution and stringent criteria [48,49]. Pinocytic vesicles (Fig. 7), for example, may (and probably have) been mistaken for viral particles. Despite these challenges, when immunohistochemical and in situ hybridization tools are lacking, EM could be considered.

2.4. Cardiotoxicities

Myriad presentations of cardiac toxicity may occur [50]. Direct causation of deleterious cardiac sequalae is challenging to demonstrate, owing to 1) the complexity of patients receiving such medications, whose polypharmacy and underlying comorbidities lead to a convoluted clinical presentation, and 2) the diverse mechanisms through which toxic affects to the myocardium may occur.

Moreover, undesirable cardiac side effects may be clinically occult at the time of pharmaceutical approval by governing agencies. Since 1955, 27 drugs have been approved and subsequently withdrawn from the market due to cardiotoxic affects that outweighed any potential benefit to the patient [51]. While some of these effects represent changes that are challenging to identify by histologic and ultrastructural means (e.g. electrophysiologic alternations), other manifestations are optimally assessed by pathologists. As such, continued vigilance is paramount as repeated instances of pharmaceutically related myocardial injury are likely to occur.

2.4.1. Doxorubicin

Perhaps one of the most prototypical examples of potential cardiac toxicity can be found in the body of literature surrounding doxorubicin. This medication falls under the classification of anthracyclines, wherein doxorubicin represents a secondary metabolite of daunorubicin, an antitumoral antibiotic derived from *Streptomyces* sp [51]. It was approved for use in the United States in 1974 under the brand name Adriamycin and lauded for its high therapeutic index and wide applicability for diverse oncologic indications [52–54].

Since that time, acute and chronic cardiac complications have been documented. Mechanistically, toxicity is attributed to multifactorial in vivo events, including free radical production and disruption of oxidative phosphorylation through inhibition of succinate dehydrogenase coenzyme Q, among others [50,55]. Chronic manifestations of doxorubicin cardiotoxicity may occur up to 15 years after original administration of the drug [51]. Most commonly, this takes the form of a dilated cardiomyopathy on echocardiography, though electrocardiographic changes and pericarditis have been documented [51]. Cardiotoxicity may be synergized by combination regimens with drugs such as trastuzumab (Herceptin) [56,57].

Histologically, myocyte hypertrophy, interstitial fibrosis, edema, and patchy myocyte vacuolization with rarefication of myofibrillar elements is apparent. Ultrastructural examination can assist not only in confirming a clinical and histologic suspicion for doxorubicin cardiotoxicity, but also in grading the degree of myocyte injury (grades 0-3) according to the amount of quality of damage present (Billingham classification [58], Table 5)[58]. EM is not technically necessary to employ this grading system; ten 1-µm thick toluidine blue-stained sections can be evaluated as an alternative approach.

Electron microscopy findings in the early stages of the process may be observed in single myocytes, juxtaposed to preserved myocardium (Fig. 19A). Sarcoplasmic vacuolization with loss of contractile elements is a common ultrastructural observation (Fig. 19B). Mitochondrial and other intra-sarcoplasmic organelles show swelling and degeneration, the former with loss of

normal cristae architecture (Fig. 19C). As the process progresses, confluent cardiomyocytes will demonstrate these changes [58].

2.4.2. Hydroxychloroquine

Hydroxychloroquine was marketed under the brand name of Plaquenil in 1955, with functional activity as an antimalarial and antirheumatic agent [59]. It represented a presumed improvement over its parent compound, chloroquine, after studies demonstrated a 40% reduction in potential toxicity following the addition of a hydroxyl group [60].

As a basic amine, hydroxychloroquine is lysosomotropic. Resultant increase in lysosome pH leads to inhibition of resident enzymes and accumulation of metabolic products [59]. The drug has also demonstrated direct binding to phospholipid membranes with subsequent calcium dysregulation.

Chronic hydroxychloroquine cardiotoxicity takes the form of biventricular hypertrophy and biatrial dilatation with diastolic and systolic dysfunction, the former outpacing the latter [61,62]. Interestingly, recognition of this process and early cessation may halt or reverse the toxic cardiac affects [62].

Histologically, prominent myocyte vacuolization is apparent, though is often not optically clear but rather has punctate, granular eosinophilic material within the distended sarcoplasm (Fig. 20A). Ultrastructural studies show a combination of myelin-like (lamellar) figures (Fig. 20B) and curvilinear bodies (Fig. 20C) [63], the latter being the more specific finding, as myelin-like figures are seen in storage diseases as well [64].

2.4.3. Other findings

A multitude of additional ultrastructural cardiac findings have been described in association with various licit and illicit drugs. Many are not specific for a single etiology, but rather reflect either temporary or permanent damage to the myocardium.

An example of this change can be found in the form of mitochondrial densities (i.e. intramitochondrial amorphous matrix densities), which are a recurrent curiosity described in multiple settings including irreversible ischemia, [65,66] following ethidium bromide administration [67], and with doxorubicin cardiotoxicity (Fig. 21) [54]. It is likely that these represent lipid-derived precipitates that accumulate following irreversible organelle injury, though a subset with central clearing and extreme electron-density may represent mitochondrial calcific deposits [65].

Additional findings such as apoptotic myocyte nuclei, cellular and organelle swelling with sarcolemmic blebs, and myofibrillolysis are regarded as non-specific patterns of myocyte injury [66,68].

While not all ultrastructural findings are pathognomonic of individual toxicities, patterns of cardiac injury have been documented in conjunction with specific medications and illicit substances. In 2021 and 2022 alone, 87 new drugs were approved by the Food and Drug Administration. Long-term complications of such treatments cannot always be predicted, calling for continued attention to potential new cardiac injury patterns in our patients.

3. Future directions

EM has undergone years of technological advances. While remaining one of the reliable tools for a small subset of cardiovascular pathology cases, the advances to using EM diagnostically have not kept pace with the technology. What follows is a glimpse into the opportunities to translate the old and new EM technologies. It is worth saying at the start, however, that electron microscopy may not be the most cost effective of interventions, and every institution would need

to assess the cost benefit of these technologies in context of their local patient population, level of care, and cost constraints. The technology, however, should not be dismissed by the price tag alone, but considered carefully for some of the unique benefits.

3.1. Immuno-electron microscopy

The use of immunohistochemistry revolutionized the practice of pathology. Increased sensitivity and specificity, as well as outright revisions to diagnostic criteria (including lots of entirely new diagnoses), became instantly available, and development and validation of new stains has become a routine component of every major pathology lab.

Immunolabeling also exists in EM, first emerging in the 1940s [69]. The principles are nearly identical, with well-established protocols [70]. Currently, the “detection reagent” for these methods is often gold particle labeling, with newer methods including peroxidase-based labels, quantum dots, and nanospheres. The latter technologies in particular are well suited for combination with spectroscopy methods (see below) for multiplex antigen labeling. The advantage of immuno-EM is that antigens poorly resolved on bright field can be formally characterized, such as subtle amyloid deposition [71], previously ill-defined structures, or myofibrillary ultrastructure (for example, altered patterns of actin, myosin, cytoskeleton, etc.).

3.2. Scanning-transmission electron microscopy (STEM)

Despite the name, scanning-transmission EM (STEM) is really a modification of TEM, less so an application of scanning EM (SEM, see below). By making modifications to the TEM instrument, additional visualization techniques become possible utilizing scattered electrons and x-rays, providing additional information beyond just the transmitted image. The applications of this for diagnostics are relatively unexplored to date but should be considered as the field progresses [72]. Devices for STEM are more likely to be adaptable to current specimens and methods than

those for SEM, although some devices now have capacity for TEM, STEM, SEM, and electron spectroscopy (EMS, see below).

3.3. EM spectroscopy

The electron beam in TEM, and also SEM, results in a significant scatter of electrons that aren't transmitted, as well as release of x-rays from the surfaces being impacted by the electrons. Various techniques exist to capture these, often in quantitative ways, more similar to x-ray spectroscopy than to the image-based TEM. This supplemental information can be digitally combined with the image data to provide extremely high depth of information [73]. One obvious application of such technologies will be imaging immune-EM with particles having defined spectroscopic characteristics, but this same can be generalized to molecular imaging independent of antibody labeling as tools become more refined.

3.4. Scanning electron microscopy (SEM)

A very different technique, typically requiring a different instrument from TEM, SEM is a method for visualizing surfaces at an ultrastructural level [74]. As pathology has built most of its approach around cut cross sections, SEM would be as much of a paradigm shift as would surface or depth-based imaging in bright field specimens. Nonetheless, it may be valuable for pathology as a field to embrace such imaging approaches as it also looks to "sectionless" imaging, deep tissue surface imaging, micro-radiology, etc. This technique is particularly well suited for combining an image with spectroscopy.

3.5. Cryo-electron microscopy

As a specimen preparation technique, ultra-cooling and vitrification of specimens allows for modifications to the above methods that can improve certain information, including resolution resulting from less tissue damage caused by the electron beam [75]. The significance of this technique in diagnostic EM is completely uncertain, but worth noting for future brainstorming.

3.6. Referral centers

Although EM laboratories can be found in many academic pathology departments, cardiovascular pathology subspecialists are uncommon. Even less common are cardiovascular pathologists with extensive diagnostic EM experience. There is an opportunity to establish criteria to identify and designate centers of excellence to function as referral centers. This task may be best undertaken by societies for ultrastructural and/or cardiovascular pathology, individually or perhaps as a collaboration.

4. Conclusion

EM interpretation is considered by many to be a lost art. While newer tools, such as immunohistochemistry, are inarguably improvements over this aging technique, they cannot provide all of the ultrastructural information that can be gleaned using EM. It is the experience of some that EM of myocardial tissue, while interesting, usually adds little to the understanding of a patient's disease [76]. Nevertheless, if we dismiss the electron microscope as a relic, we will be unprepared for the rare instances in which a specific diagnosis depends on the recognition of ultrastructural pathology.

References

[1] Bozzola J, Russell L. Electron Microscopy: Principles and Techniques for Biologists. 2nd ed. Boston: Jones & Bartlett Publishers; 1998.

[2] Graham L, Orenstein JM. Processing tissue and cells for transmission electron microscopy in diagnostic pathology and research. Nat Protoc 2007;2. https://doi.org/10.1038/nprot.2007.304.

[3] Swedlow DB, Frasca P, Harper RA, Katz JL. Scanning and Transmission Electron Microscopy of Calcified Tissues*,†. Biomater Med Devices Artif Organs 1975;3:121–53. https://doi.org/10.3109/10731197509118617.

[4] Tsutsumi Y. Electron Microscopic Study Using Formalin-fixed, Paraffin-embedded Material, with Special Reference to Observation of Microbial Organisms and Endocrine Granules. Acta Histochem Cytochem 2018;51:63–71. https://doi.org/10.1267/ahc.18012.

[5] Ayache J, Beaunier L, Boumendil J, Ehret G, Laub D. Artifacts in Transmission Electron Microscopy. In: Ayache J, Beaunier L, Boumendil J, Ehret G, Laub D, editors. Sample Preparation Handbook for Transmission Electron Microscopy: Methodology, New York, NY: Springer New York; 2010, p. 125–70. https://doi.org/10.1007/978-0-387-98182-6_6.

[6] Crocini C, Gotthardt M. Cardiac sarcomere mechanics in health and disease. Biophys Rev 2021;13. https://doi.org/10.1007/s12551-021-00840-7.

[7] Maleszewski J, Lai C, Nair V, Veinot J. Anatomic considerations and examination of cardiovascular specimens (excluding devices). In: Buja L, Butany J, editors. Cardiovascular Pathology. 5th ed., Academic Press; 2022, p. 27–84.

[8] Weiss L, editor. Cell and tissue biology. A textbook of histology. . 6th ed. 1988.

[9] Zhao G, Qiu Y, Zhang HM, Yang D. Intercalated discs: cellular adhesion and signaling in heart health and diseases. Heart Fail Rev 2019;24:115–32. https://doi.org/10.1007/s10741-018-9743-7.

[10] Gerdes AM. Cardiomyocyte Ultrastructure. Muscle, vol. 1, Elsevier; 2012, p. 47–55. https://doi.org/10.1016/B978-0-12-381510-1.00005-3.

[11] Park SY, Gifford JR, Andtbacka RHI, Trinity JD, Hyngstrom JR, Garten RS, et al. Cardiac, skeletal, and smooth muscle mitochondrial respiration: Are all mitochondria created equal? Am J Physiol Heart Circ Physiol 2014;307:346–52. https://doi.org/10.1152/AJPHEART.00227.2014/ASSET/IMAGES/LARGE/ZH401514120200004.JPEG.

[12] Kakimoto Y, Okada C, Kawabe N, Sasaki A, Tsukamoto H, Nagao R, et al. Myocardial lipofuscin accumulation in ageing and sudden cardiac death. Sci Rep 2019;9. https://doi.org/10.1038/s41598-019-40250-0.

[13] Legato MJ. Ultrastructure of the atrial, ventricular, and Purkinje cell, with special reference to the genesis of arrhythmias. Circulation 1973;47. https://doi.org/10.1161/01.CIR.47.1.178.

[14] Yang H, Borg TK, Wang Z, Ma Z, Gao BZ. Role of the basement membrane in regulation of cardiac electrical properties. Ann Biomed Eng 2014;42. https://doi.org/10.1007/s10439-014-0992-x.

[15] McDowell EM, Trump BF. Histologic fixatives suitable for diagnostic light and electron microscopy. Arch Pathol Lab Med 1976;100:405–14.

[16] Ashworth M. Metabolic and Storage Disease. Pathology of Heart Disease in the Fetus, Infant and Child, Cambridge University Press; 2019, p. 221–42. https://doi.org/10.1017/9781316337073.010.

[17] Wicks EC, Elliott · P M. Genetics and metabolic cardiomyopathies. Herz 2012;37:598–611. https://doi.org/10.1007/s00059-012-3659-0.

[18] Gandjbakhch E, Redheuil A, Pousset F, Charron P, Frank R. Clinical Diagnosis, Imaging, and Genetics of Arrhythmogenic Right Ventricular Cardiomyopathy/Dysplasia: JACC State-of-the-Art Review. J Am Coll Cardiol 2018;72. https://doi.org/10.1016/j.jacc.2018.05.065.

[19] Kaplan SR, Gard JJ, Protonotarios N, Tsatsopoulou A, Spiliopoulou C, Anastasakis A, et al. Remodeling of myocyte gap junctions in arrhythmogenic right ventricular cardiomyopathy due to a deletion in plakoglobin (Naxos disease). Heart Rhythm 2004;1:3–11. https://doi.org/10.1016/j.hrthm.2004.01.001.

[20] Fujita S, Terasaki F, Otsuka K, Katashima T, Kanzaki Y, Kawamura K, et al. Markedly increased intracellular lipid droplets and disruption of intercellular junctions in biopsied myocardium from a patient with arrhythmogenic right ventricular cardiomyopathy. Heart Vessels 2008;23. https://doi.org/10.1007/s00380-008-1079-0.

[21] Basso C, Czarnowska E, Barbera M Della, Bauce B, Beffagna G, Wlodarska EK, et al. Ultrastructural evidence of intercalated disc remodelling in arrhythmogenic right ventricular cardiomyopathy: An electron microscopy investigation on endomyocardial biopsies. Eur Heart J 2006;27. https://doi.org/10.1093/eurheartj/ehl095.

[22] Lorenzon A, Beffagna G, Bauce B, De Bortoli M, Li Mura IEA, Calore M, et al. Desmin Mutations and Arrhythmogenic Right Ventricular Cardiomyopathy. Am J Cardiol 2013;111:400. https://doi.org/10.1016/J.AMJCARD.2012.10.017.

[23] McLendon PM, Robbins J. Desmin-related cardiomyopathy: an unfolding story. Am J Physiol Heart Circ Physiol 2011;301:H1220-8. https://doi.org/10.1152/ajpheart.00601.2011.

[24] Kubánek M, Schimerová T, Piherová L, Brodehl A, Krebsová A, Ratnavadivel S, et al. Desminopathy: Novel desmin variants, a new cardiac phenotype, and further evidence for secondary mitochondrial dysfunction. J Clin Med 2020;9. https://doi.org/10.3390/jcm9040937.

[25] Ferrans VJ, Rodriguez ER. Specificity of light and electron microscopic features of hypertrophic obstructive and nonobstructive cardiomyopathy. Qualitative, quantitative and etiologic aspects. Eur Heart J 1983;4. https://doi.org/10.1093/eurheartj/4.suppl_f.9.

[26] Nollet EE, Duursma I, Rozenbaum A, Eggelbusch M, Wüst RCI, Schoonvelde SAC, et al. Mitochondrial dysfunction in human hypertrophic cardiomyopathy is linked to cardiomyocyte architecture disruption and corrected by improving NADH-driven mitochondrial respiration. Eur Heart J 2023;44. https://doi.org/10.1093/eurheartj/ehad028.

[27] Ranjbarvaziri S, Kooiker KB, Ellenberger M, Fajardo G, Zhao M, Vander Roest AS, et al. Altered Cardiac Energetics and Mitochondrial Dysfunction in Hypertrophic Cardiomyopathy. Circulation 2021;144. https://doi.org/10.1161/CIRCULATIONAHA.121.053575.

[28] Hasselberg NE, Haland TF, Saberniak J, Brekke PH, Berge KE, Leren TP, et al. Lamin A/C cardiomyopathy: Young onset, high penetrance, and frequent need for heart transplantation. Eur Heart J 2018;39. https://doi.org/10.1093/eurheartj/ehx596.

[29] Arbustini E, Pilotto A, Repetto A, Grasso M, Negri A, Diegoli M, et al. Autosomal dominant dilated cardiomyopathy with atrioventricular block: a lamin A/C defect-related disease. J Am Coll Cardiol 2002;39:981–90. https://doi.org/10.1016/S0735-1097(02)01724-2.

[30] Diercks GF, Van Tintelen JP, Tio RA, Kerstjens-Frederikse WS, Pinto YM, Suurmeijer AJ. Ultrastructural pathology of the nuclear envelope in familial lamin A/C cardiomyopathy. Cardiovascular Pathology 2010;19. https://doi.org/10.1016/j.carpath.2009.03.001.

[31] Herman DS, Lam L, Taylor MRG, Wang L, Teekakirikul P, Christodoulou D, et al. Truncations of Titin Causing Dilated Cardiomyopathy. New England Journal of Medicine 2012;366:619–28. https://doi.org/10.1056/NEJMOA1110186/SUPPL_FILE/NEJMOA1110186_DISCLOSURES.PDF.

[32] Maleszewski JJ. Cardiac amyloidosis: pathology, nomenclature, and typing. Cardiovascular Pathology 2015;24:343–50. https://doi.org/10.1016/j.carpath.2015.07.008.

[33] Eletta O, Ali M, Grieff A, Puri S, Matsuda K, Bongu A, et al. Clinically occult amyloidosis derived from leukocyte chemotactic factor 2 (ALECT 2) with cardiac involvement complicating renal transplantation: case report and literature review. Cardiovascular Pathology 2021;55:107375. https://doi.org/10.1016/J.CARPATH.2021.107375.

[34] Sipe JD, Cohen AS. Review: History of the Amyloid Fibril. J Struct Biol 2000;130:88–98. https://doi.org/10.1006/JSBI.2000.4221.

[35] Siadat SM, Silverman AA, DiMarzio CA, Ruberti JW. Measuring Collagen Fibril Diameter with Differential Interference Contrast Microscopy. J Struct Biol 2021;213:107697. https://doi.org/10.1016/J.JSB.2021.107697.

[36] Osanami A, Yano T, Takemura G, Ikeda H, Inyaku M, Toda Y, et al. Cardiac Light Chain Deposition Disease Mimicking Immunoglobulin Light Chain Amyloidosis: Two Branches of the Same Tree. Circ Cardiovasc Imaging 2020:1–3. https://doi.org/10.1161/CIRCIMAGING.120.010478.

[37] Linder J, Croker BP, Vollmer RT, Shelburne J. Systemic kappa light-chain deposition. An ultrastructural and immunohistochemical study. Am J Surg Pathol 1983;7:85–93. https://doi.org/10.1097/00000478-198301000-00009.

[38] Kunnath-Velayudhan S, Larsen BT, Coley SM, De Michele S, Santoriello D, Colby T V., et al. Masson Trichrome and Sulfated Alcian Blue Stains Distinguish Light Chain Deposition Disease From Amyloidosis in the Lung. American Journal of Surgical Pathology 2021;45:405–13. https://doi.org/10.1097/PAS.0000000000001593.

[39] Nishioka R, Yoshida S, Takamatsu H, Kawano M. Cardiac light-chain deposition disease and hints at diagnosing: a case report. Eur Heart J Case Rep 2023;7:1–7. https://doi.org/10.1093/EHJCR/YTAD049.

[40] https://www.scvp.net/electron-microscopy-tutorial/#light-chain-deposition-disease 2024.

[41] Buja LM, Roberts WC. Iron in the heart. Am J Med 1971;51:209–21. https://doi.org/10.1016/0002-9343(71)90240-3.

[42] Kremastinos DT, Farmakis D, Aessopos A, Hahalis G, Hamodraka E, Tsiapras D, et al. Beta-thalassemia cardiomyopathy: history, present considerations, and future perspectives. Circ Heart Fail 2010;3:451–8. https://doi.org/10.1161/CIRCHEARTFAILURE.109.913863.

[43] Pietrangelo A. Hereditary Hemochromatosis — A New Look at an Old Disease. New England Journal of Medicine 2004;350:2383–97. https://doi.org/10.1056/NEJMra031573.

[44] Sanyal SK, Johnson W, Jayalakshmamma B, Green AA. Fatal “iron heart” in an adolescent: biochemical and ultrastructural aspects of the heart. Pediatrics 1975;55:336–41.

[45] Hübner G. Electron Microscopic Demonstration of Viruses in the Myocardium, with Particular Reference to Reovirus. Viral Heart Disease, Springer; 1984, p. 31–4.

[46] Tavazzi G, Pellegrini C, Maurelli M, Belliato M, Sciutti F, Bottazzi A, et al. Myocardial localization of coronavirus in COVID-19 cardiogenic shock. Eur J Heart Fail 2020;22:911–5. https://doi.org/10.1002/EJHF.1828.

[47] Fox SE, Li G, Akmatbekov A, Harbert JL, Lameira FS, Brown JQ, et al. Unexpected Features of Cardiac Pathology in COVID-19 Infection. Circulation 2020;142:1123–5. https://doi.org/10.1161/CIRCULATIONAHA.120.049465.

[48] Dittmayer C, Meinhardt J, Radbruch H, Radke J, Heppner BI, Heppner FL, et al. Why misinterpretation of electron micrographs in SARS-CoV-2-infected tissue goes viral. The Lancet 2020;396:e64–5. https://doi.org/10.1016/S0140-6736(20)32079-1.

[49] Hopfer H, Herzig MC, Gosert R, Menter T, Hench J, Tzankov A, et al. Hunting coronavirus by transmission electron microscopy – a guide to SARS-CoV-2-associated ultrastructural pathology in COVID-19 tissues. Histopathology 2021;78:358–70. https://doi.org/10.1111/HIS.14264.

[50] Combs AB, Acosta D. Toxic mechanisms of the heart: A review. Toxicol Pathol, vol. 18, 1990. https://doi.org/10.1177/019262339001804a08.

[51] Octavia Y, Tocchetti CG, Gabrielson KL, Janssens S, Crijns HJ, Moens AL. Doxorubicin-induced cardiomyopathy: From molecular mechanisms to therapeutic strategies. J Mol Cell Cardiol 2012;52. https://doi.org/10.1016/j.yjmcc.2012.03.006.

[52] Renu K, V.G. A, Tirupathi TP, Arunachalam S. Molecular mechanism of doxorubicin-induced cardiomyopathy – An update. Eur J Pharmacol 2018;818. https://doi.org/10.1016/j.ejphar.2017.10.043.

[53] Bo L, Wang Y, Li Y, Wurpel JND, Huang Z, Chen ZS. The Battlefield of Chemotherapy in Pediatric Cancers. Cancers (Basel) 2023;15. https://doi.org/10.3390/cancers15071963.

[54] Lefrak EA, Piťha J, Rosenheim S, Gottlieb JA. A clinicopathologic analysis of adriamycin cardiotoxicity. Cancer 1973;32. https://doi.org/10.1002/1097-0142(197308)32:2<302::AID-CNCR2820320205>3.0.CO;2-2.

[55] Gammella E, Maccarinelli F, Buratti P, Recalcati S, Cairo G. The role of iron in anthracycline cardiotoxicity. Front Pharmacol 2014;5 FEB. https://doi.org/10.3389/fphar.2014.00025.

[56] Thavendiranathan P, Abdel-Qadir H, Fischer HD, Camacho X, Amir E, Austin PC, et al. Breast Cancer therapy-related cardiac dysfunction in adult women treated in routine clinical practice: A population-based cohort study. Journal of Clinical Oncology 2016;34:2239–46. https://doi.org/10.1200/JCO.2015.65.1505/ASSET/IMAGES/LARGE/JCO651505T4.JPEG.

[57] Jiang J, Mohan N, Endo Y, Shen Y, Wu WJ. Type IIB DNA topoisomerase is downregulated by trastuzumab and doxorubicin to synergize cardiotoxicity. Oncotarget 2018;9:6095. https://doi.org/10.18632/ONCOTARGET.23543.

[58] Billingham ME, Mason JW, Bristow MR, Daniels JR. Anthracycline cardiomyopathy monitored by morphologic changes. Cancer Treat Rep 1978;62.

[59] Yogasundaram H, Putko BN, Tien J, Paterson DI, Cujec B, Ringrose J, et al. Hydroxychloroquine-Induced Cardiomyopathy: Case Report, Pathophysiology, Diagnosis, and Treatment. Canadian Journal of Cardiology 2014;30. https://doi.org/10.1016/j.cjca.2014.08.016.

[60] Lebin JA, LeSaint KT. Brief review of chloroquine and hydroxychloroquine toxicity and management. Western Journal of Emergency Medicine 2020;21. https://doi.org/10.5811/westjem.2020.5.47810.

[61] Manohar VA, Moder KG, Edwards WD, Klarich K. Restrictive cardiomyopathy secondary to hydroxychloroquine therapy. Journal of Rheumatology 2009;36. https://doi.org/10.3899/jrheum.080305.

[62] Yogasundaram H, Hung W, Paterson ID, Sergi C, Oudit GY. Chloroquine-induced cardiomyopathy: a reversible cause of heart failure. ESC Heart Fail 2018;5. https://doi.org/10.1002/ehf2.12276.

[63] Tönnesmann E, Kandolf R, Lewalter T. Chloroquine cardiomyopathy-a review of the literature. Immunopharmacol Immunotoxicol 2013;35. https://doi.org/10.3109/08923973.2013.780078.

[64] Roos JM, Aubry MC, Edwards WD. Chloroquine cardiotoxicity: Clinicopathologic features in three patients and comparison with three patients with Fabry disease. Cardiovascular Pathology 2002;11:277–83. https://doi.org/10.1016/S1054-8807(02)00118-7.

[65] Trump B, Jones R. Diagnostic Electron Microscopy. vol. 4. John Wiley & Sons, Inc.; 1983.

[66] Collins HE, Kane MS, Litovsky SH, Darley-Usmar VM, Young ME, Chatham JC, et al. Mitochondrial Morphology and Mitophagy in Heart Diseases: Qualitative and Quantitative Analyses Using Transmission Electron Microscopy. Frontiers in Aging 2021;2:1–22. https://doi.org/10.3389/fragi.2021.670267.

[67] McGill M, Hsu TC, Brinkley BR. Electron-dense structures in mitochondria induced by short-term ethidium bromide treatment. Journal of Cell Biology 1973;59. https://doi.org/10.1083/jcb.59.1.260.

[68] Frustaci A, Russo MA, Morgante E, Scopelliti F, Aquilano K, Ciriolo MR, et al. Oxidative myocardial damage in human cocaine-related cardiomyopathy. Eur J Heart Fail 2015;17. https://doi.org/10.1002/ejhf.231.

[69] Anderson TF, Stanley WM. A study by means of the electron microscope of the reaction between tobacco mosaic virus and its antiserum. Journal of Biological Chemistry 1941;139:339–44.

[70] Aishwarya R, Abdullah CS, Remex NS, Nitu S, Hartman B, King J, et al. Visualizing Subcellular Localization of a Protein in the Heart using Quantum Dots-Mediated Immuno-Labeling followed by Transmission Electron Microscopy. J Vis Exp 2022;2022. https://doi.org/10.3791/64085.

[71] Abildgaard N, Rojek AM, Møller HEH, Palstrøm NB, Nyvold CG, Rasmussen LM, et al. Immunoelectron microscopy and mass spectrometry for classification of amyloid deposits. Amyloid 2020;27:59–66. https://doi.org/10.1080/13506129.2019.1688289.

[72] Cohen Hyams T, Mam K, Killingsworth MC. Scanning electron microscopy as a new tool for diagnostic pathology and cell biology. Micron 2020;130. https://doi.org/10.1016/J.MICRON.2019.102797.

[73] Novaes RD, Maldonado IRSC, Natali AJ, Neves CA, Talvani A. Elemental mapping of cardiac tissue by scanning electron microscopy and energy dispersive X-ray spectroscopy: proof of principle in Chaga's disease myocarditis model. Can J Cardiol 2013;29:639.e3-639.e4. https://doi.org/10.1016/J.CJCA.2013.01.004.

[74] Kanzaki Y, Yamauchi Y, Okabe M, Terasaki F, Ishizaka N. Three-dimensional architecture of cardiomyocytes and connective tissues in hypertrophic cardiomyopathy: a scanning electron microscopic observation. Circulation 2012;125:738–9. https://doi.org/10.1161/CIRCULATIONAHA.111.054668.

[75] Wang Z, Grange M, Wagner T, Kho AL, Gautel M, Raunser S. The molecular basis for sarcomere organization in vertebrate skeletal muscle. Cell 2021;184:2135-2150.e13. https://doi.org/10.1016/J.CELL.2021.02.047.

[76] Mudhar HS, Wagner BE, Suvarna SK. Electron microscopy of myocardial tissue. A nine year review. J Clin Pathol 2001;54:321–5. https://doi.org/10.1136/jcp.54.4.321.

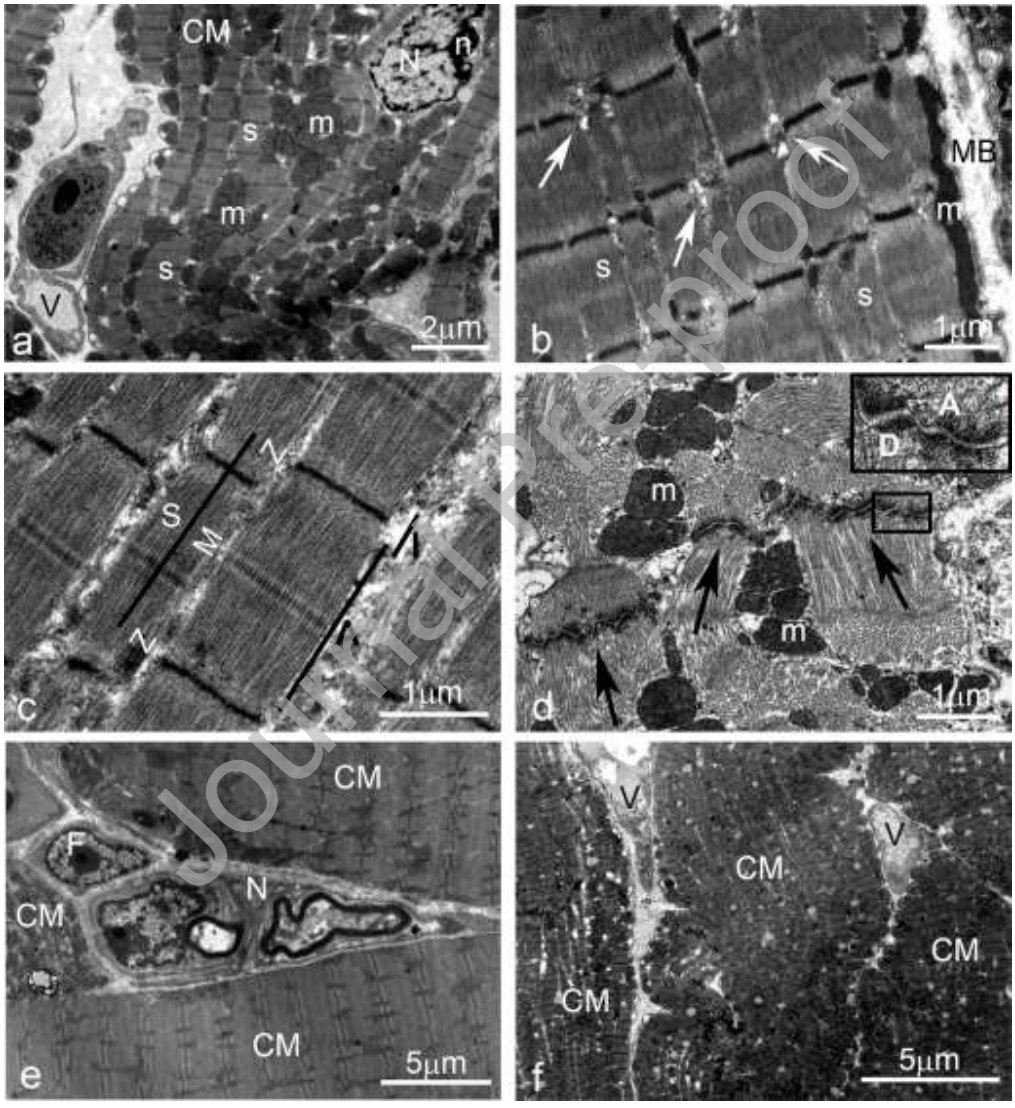

Figure 1. Normal ultrastructure of cardiac tissue

a) Low magnification of ventricular cardiomyocytes (CM): sarcomeres (s) and mitochondria (m) are visible in the cytoplasm. The nucleus (N) is oval, with a well-organized nucleolus (n). Vessels (V) are also visible in the interstitium.

b) The sarcoplasm is packed with well-organized sarcomeres (s). T-tubules (white arrows) are located among the sarcomeres. Cardiomyocytes are surrounded by a well-organized basal membrane (MB). m: mitochondria

c) High magnification of cardiac sarcomeres (s), were Z and M-lines and I and A-bands are well organized.

d) Well developed intercalated discs (black arrows) connecting end-to-end consecutive ventricular cardiomyocytes. Desmosomes (D) and adherens junctions (A) are highlighted in the insert. m: mitochondria

e) Fibroblasts (F) and nervous cells (N) are visible in the myocardium interstitium. CM: cardiomyocyte

f) Endothelial cells forming small vessels (V), are visible in the myocardium interstitium. CM: cardiomyocyte.

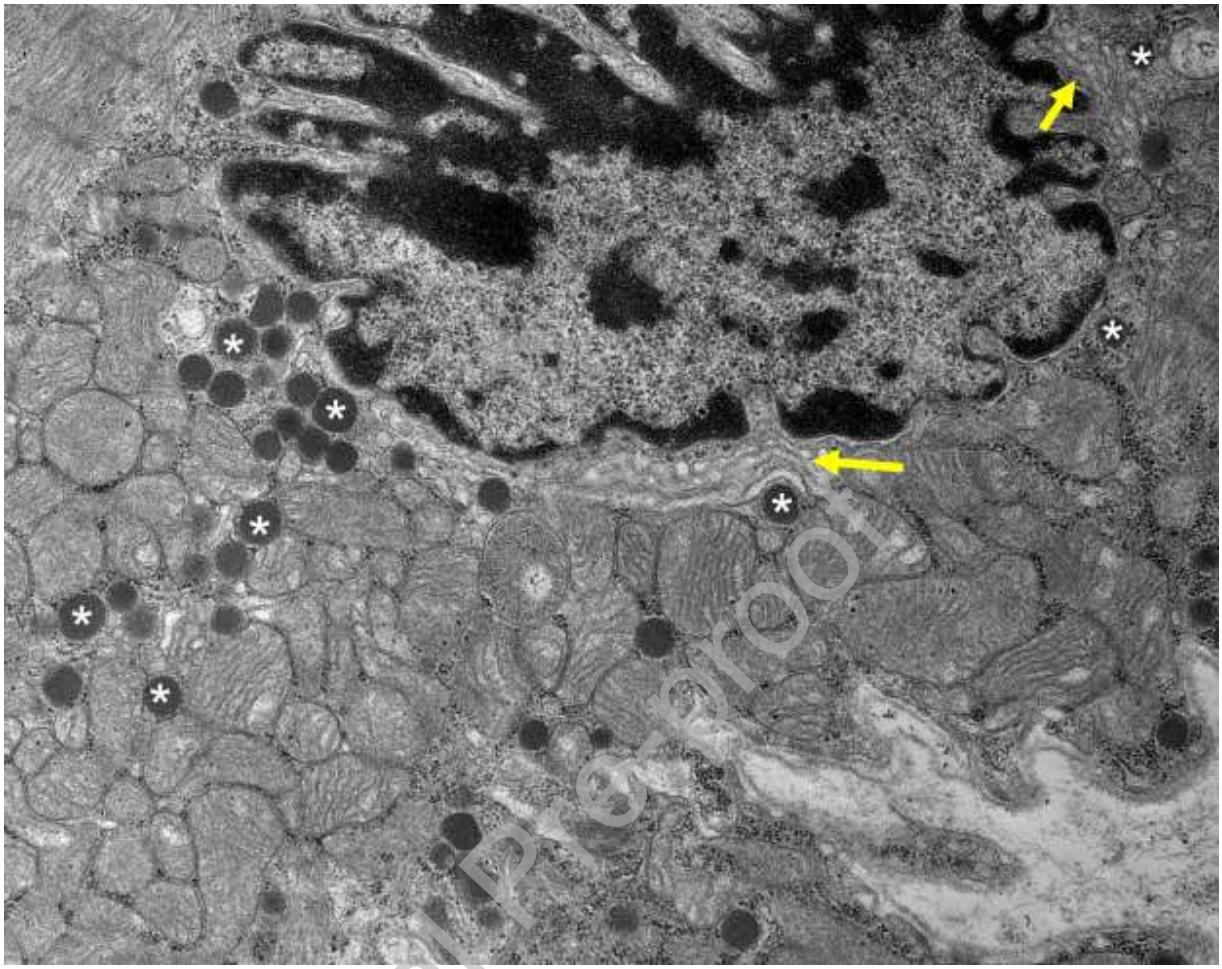

Figure 2. Atrial cardiomyocytes

An atrial cardiomyocyte containing numerous dense secretory granules (asterisks) in the perinuclear region and close to the Golgi apparatus (arrows) – a complex membrane formation with conspicuous interdigitations.

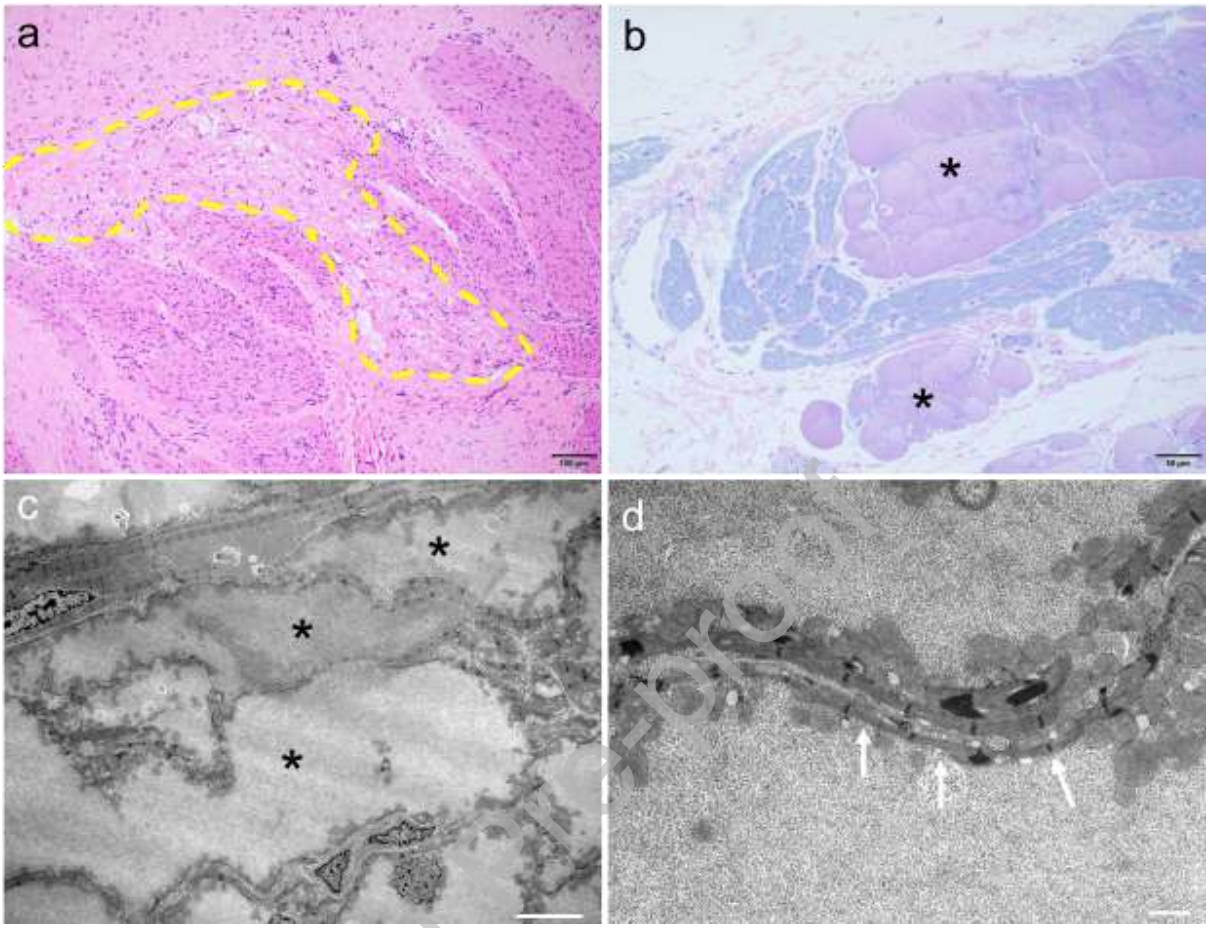

Figure 3. Purkinje cells

Atrial septal biopsy from a 3-month-old boy. Purkinje fibers (a, yellow region) comprised of large cells with pale or clear cytoplasm are present amid the contractile atrial cardiomyocytes (H&E, bar = 100 µm). Intracytoplasmic glycogen stains lavender with toluidine blue (b, bar = 50 µm). Ultrastructurally, abundant glycogen particles (*) can be seen in the sarcoplasm along with mitochondria and linearly arranged sarcomeres (white arrows) that often, but not exclusively, line the periphery of cells imparting an undulating contour (c, bar = 8 µm; d, bar = 1 µm).

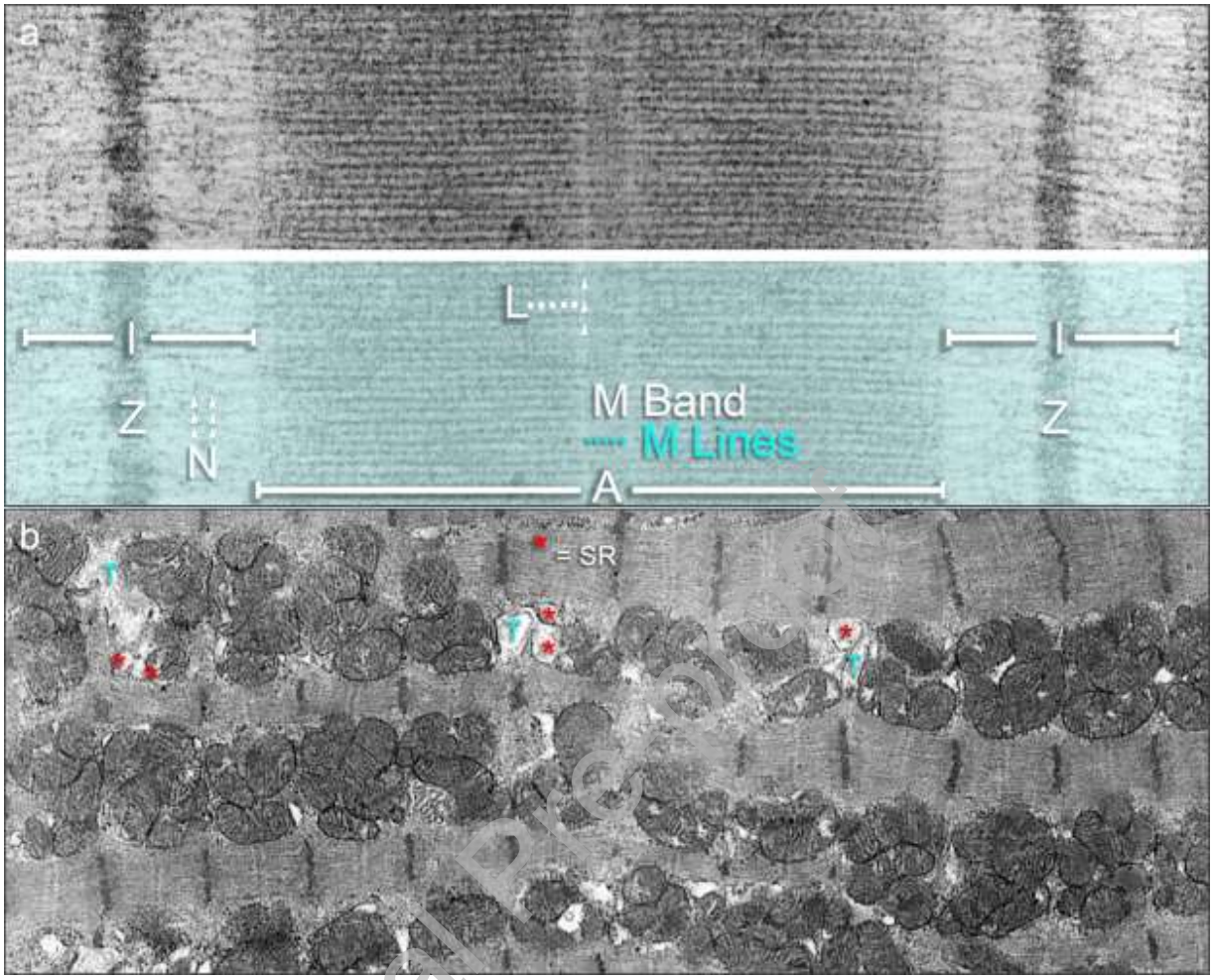

Figure 4. The sarcomere in detail

a) The **A**-band is the wide central electron dense band in the center of the sarcomere. It is bisected by the **M**-band, showing 5 fine divisions (M-lines) of alternating electron dense and electron lucent material (blue dots).The **L**-line is present at each side of the **M**-band. The sarcomere is delimited by the two **Z**-bands that bisect the **I**-band. The **N**-line bisects each half of the **I**-band. b) The sarcomeres are contracted. Approximately two mitochondria per sarcomere are present. The T-Tubules (T) are marked and show distinct electron dense material in their lumina which is similar in density to the basal lamina of the myocytes. The sarcoplasmic reticulum is marked by asterisks. One or two tubules or sarcoplasmic reticulum are seen adjacent to the T-tubules, thus forming diads and triads.

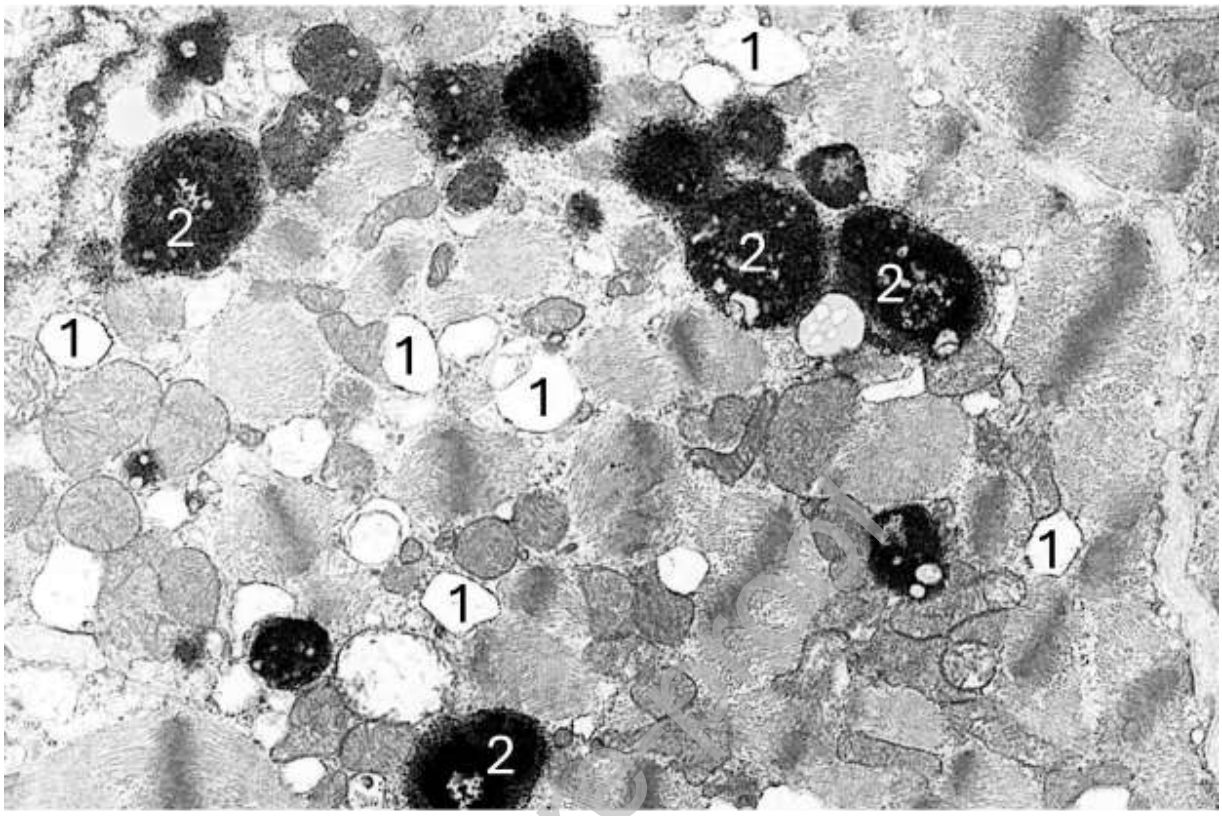

Figure 5. Lysosomes

Double membrane bound lysosomes (~200 nm, #1) and secondary lysosomes (>500 nm, #2) (dark electron-dense), also called lipofuscin granules, are present in this myocyte.

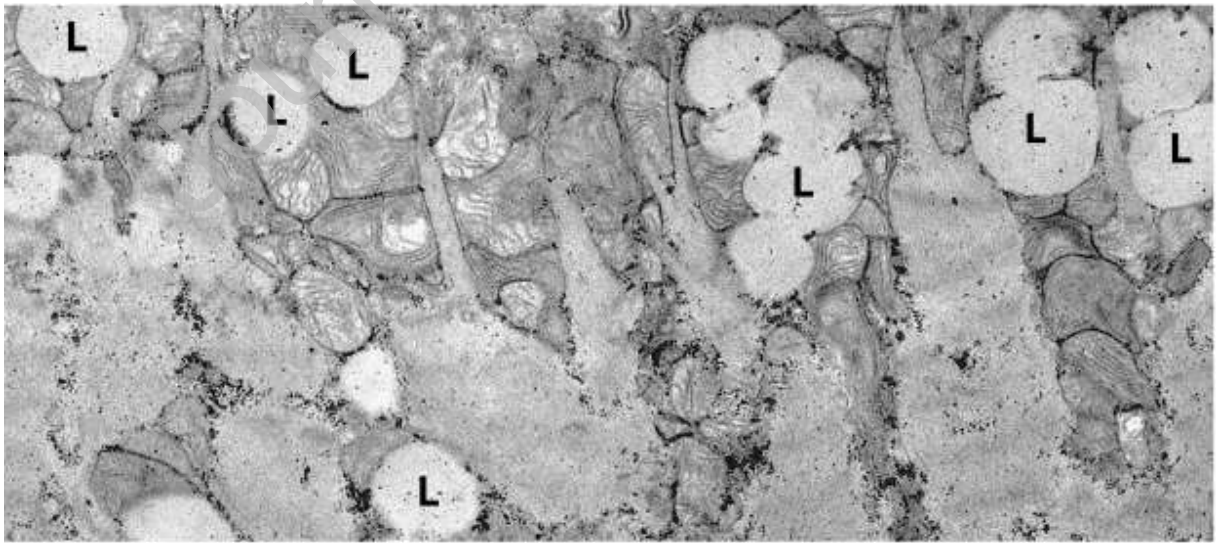

Figure 6. Lipid vacuoles

Abundant round, membrane bound slightly electron dense (compared to the lysosomes in Figure 5) lipid vacuoles (L) or droplets are present in the sarcoplasm of this myocyte. These vacuoles are similar in size to the mitrochondria present (500 nm)

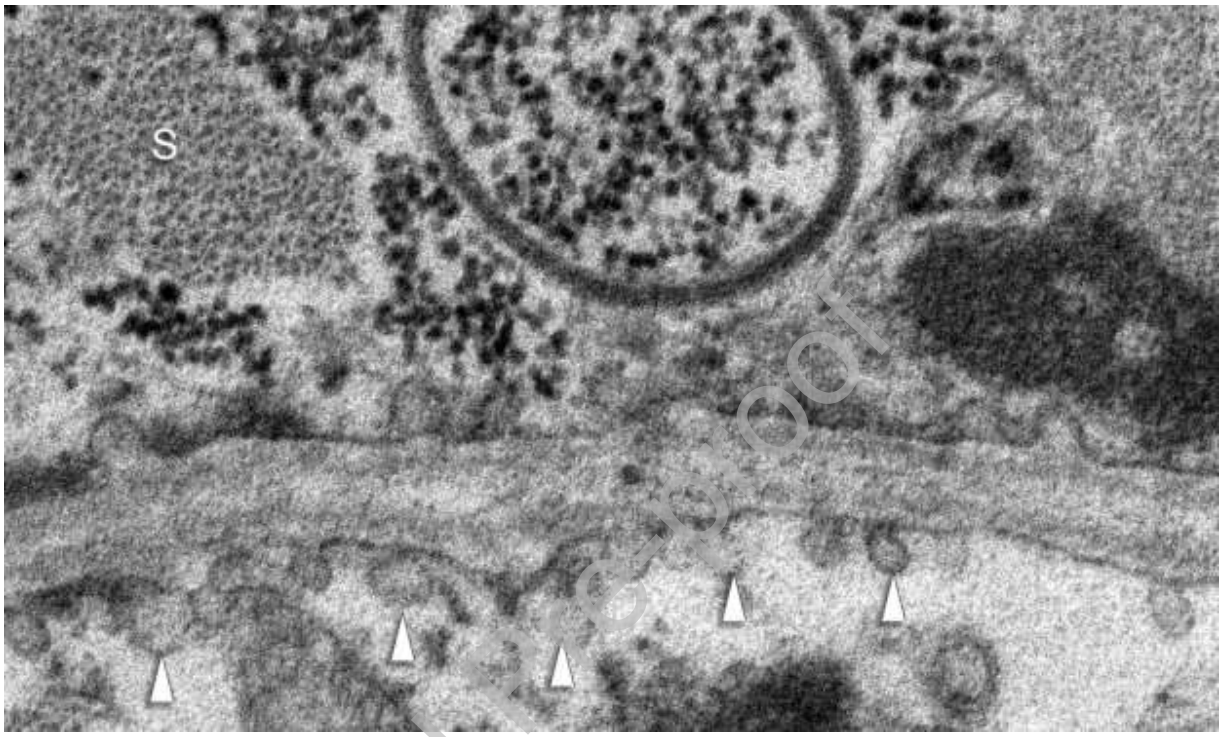

Figure 7. Pinocytic vesicles

Pinocytic vesicles are seen near the sarcolemma of two myocytes The arrowheads point a some vesicles. Similar vesicles are present in the opposite myocyte. Note the round electrondense glycogen particles and the cross section through the A-band of a sarcomere (S).

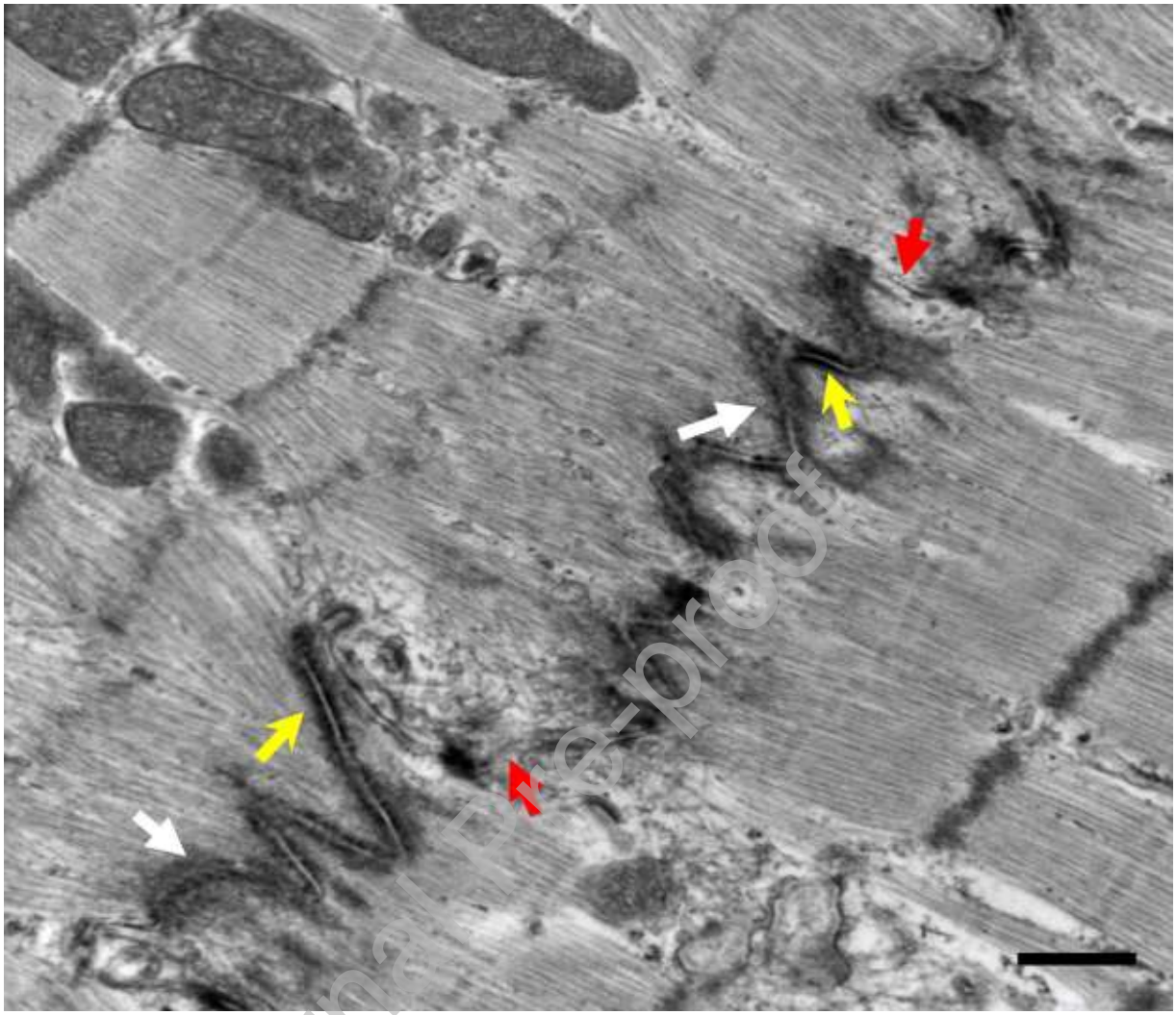

Figure 8. Intercalated discs

Intercalated discs appear as complex folded structures between cardiomyocytes. There is no Z-disc at the end of the terminal sarcomere of the myofibril. Thin filaments (actin) link into adherens junctions (white arrow), that appear dense but somewhat fuzzy and are found at the end of the myofibrils. Desmosomes (yellow arrow), in contrast, appear as dense but well-ordered structures, usually where the membrane is straight. Two adjacent cell membranes come close together and seemingly overlap at gap junctions (red arrow; bar = 600 nm).

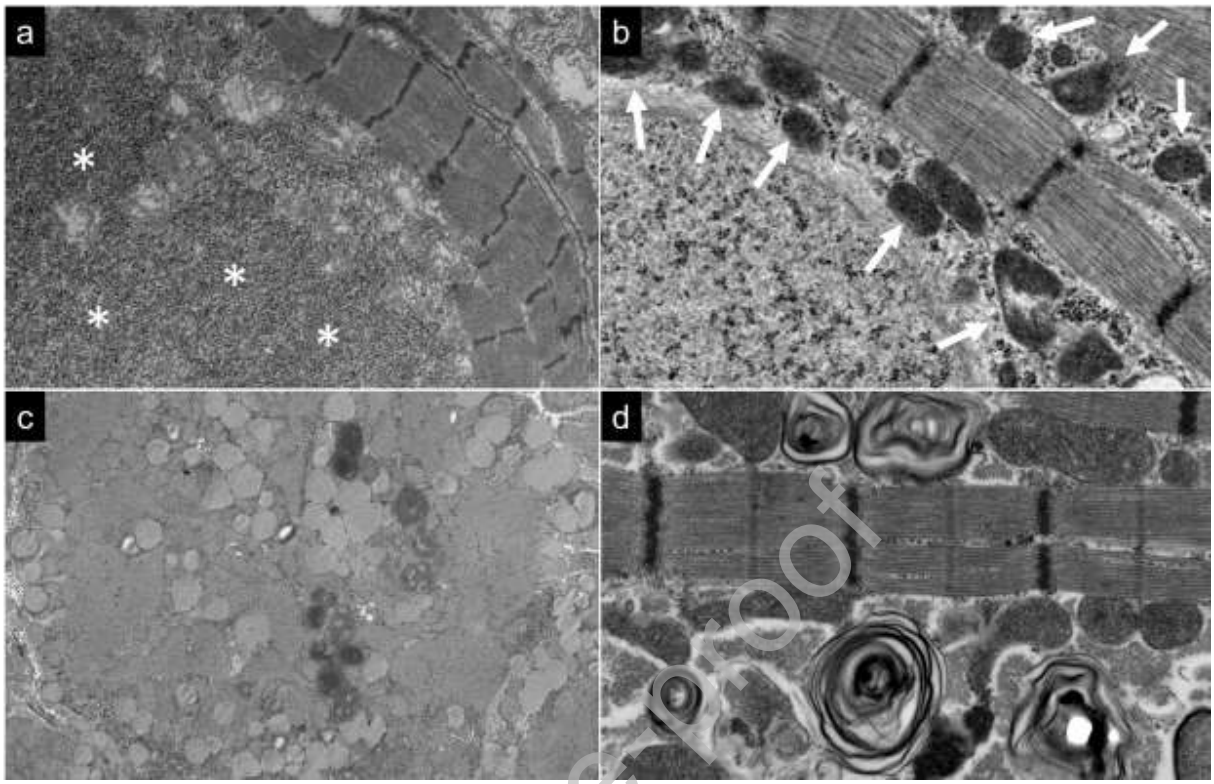

Figure 9. Storage diseases

a) Sarcoplasmic free glycogen (asterisks) in a patient with *PRKAG2* mutation. b) Glycogen storage in a double membrane bound lysosome (white arrows) adjacent to a myofibril in Pompe disease. Note the presence of dark electron-dense glycogen α-particles within the lysosome and also in the sarcoplasm next to the mitochondria and between the sarcomeres. c) Microvesicular steatosis in a patient with lysosomal storage disease--numerous lysosomes filled with lipid (lipid vacuoles) (moderately electron-dense in comparison to the lipofuscin secondary lysosomes). d) In this example of Fabry's disease, cardiac sarcomeres are surrounded by electron-dense multilamellar myelin-like figures. Some excess sarcoplasmic glycogen is also present. Note the 1-2 mitochondria per sarcomere unit ratio.

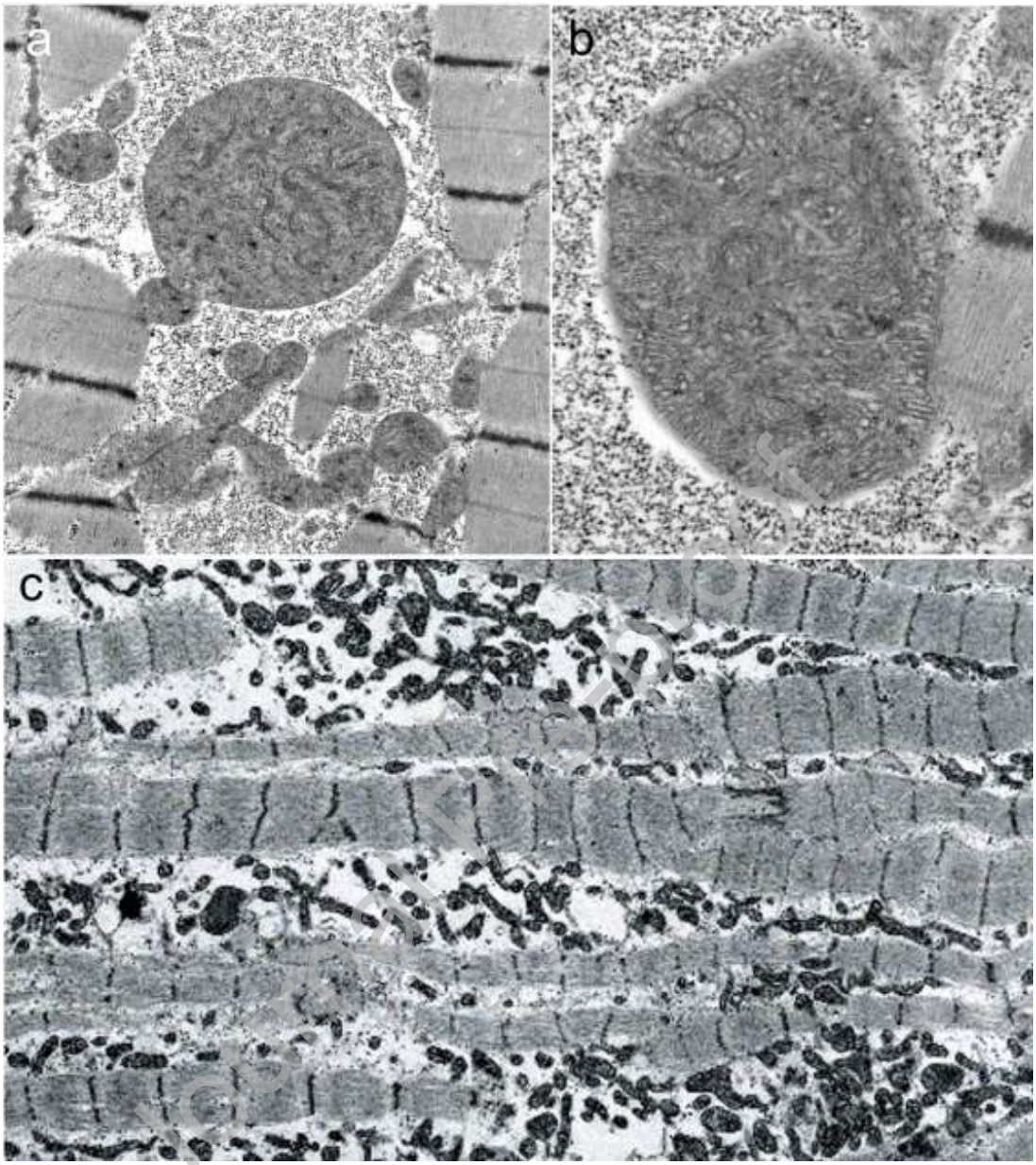

Figure 10. Mitochondrial disorders

a) Mitochondria with pleoconia (pleomorphism) and megaconia (enlargement) in a mitochondrial cardiomyopathy. b) The mitochondrial cristae no longer form the normal parallel arrays that are perpendicular to the long axis, but rather make circular arrangements that resemble fingerprints. c) In this example of a mitochondrial disorder, the ratio of 1 or 2 mitochondria per sarcomere is distinctly altered with many mitochondria per sarcomere unit. The increased number of

mitochondrial separates the myofibrils. Note that there is no contraction band artifact present, thus ruling out an artifactual conglomerate of mitochondria.

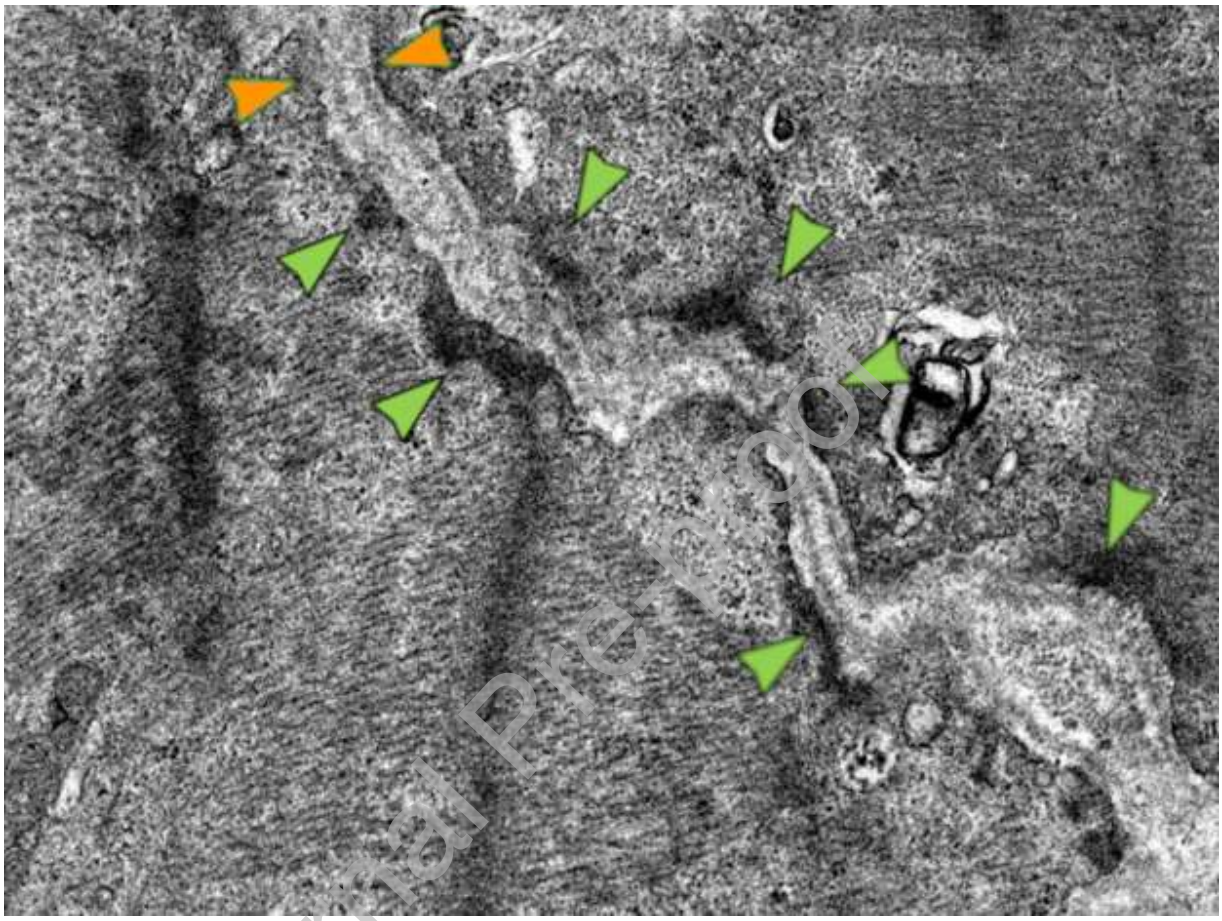

Figure 11. Arrhythmogenic cardiomyopathy

Intercalated disc in a heart with arrhythmogenic cardiomyopathy. The intercellular space is widened (orange arrowheads), and the hemidesmosomes (green arrowheads) do not align across the intercellular junction.

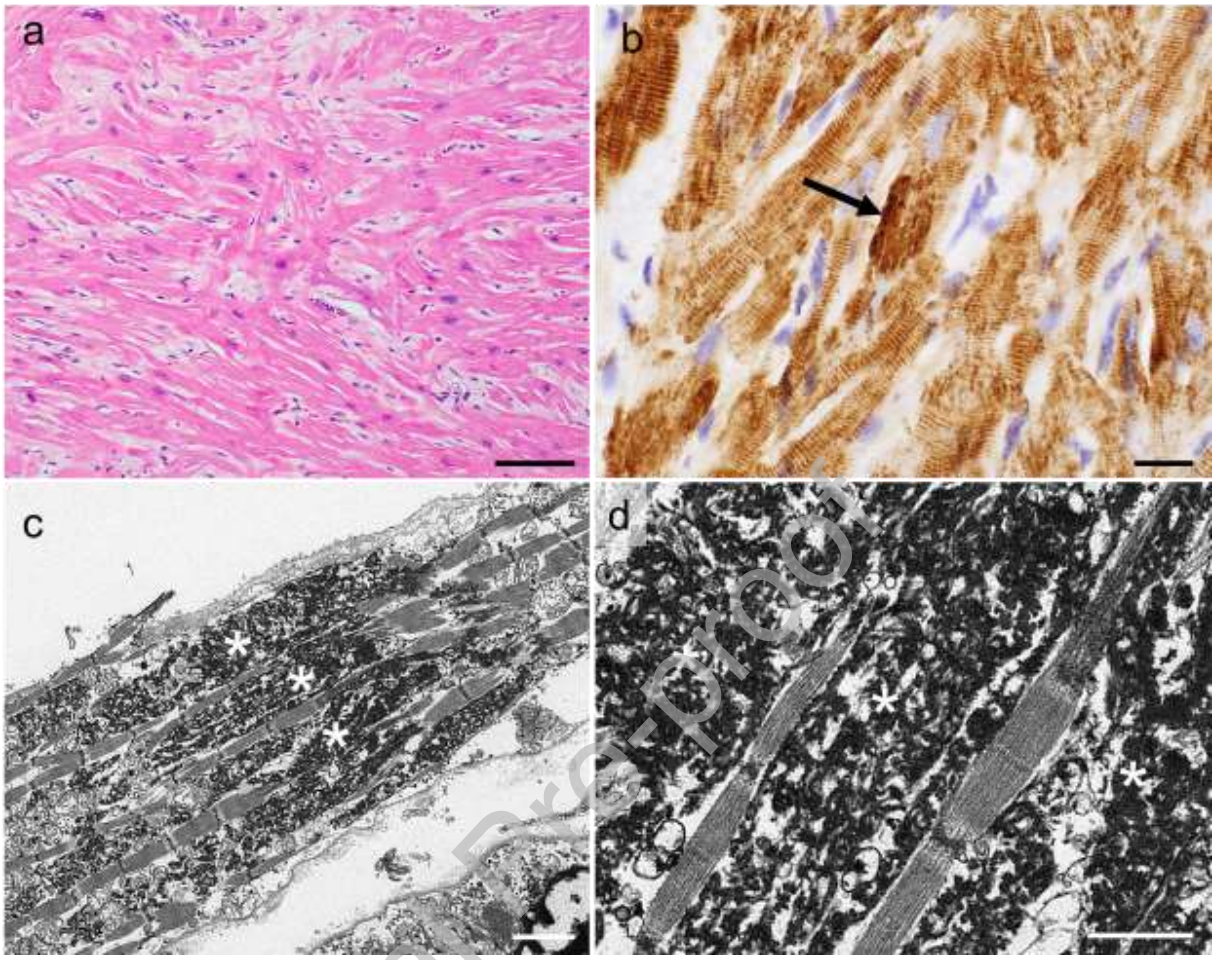

Figure 12. Desmin-related myofibrillar myopathy

Microscopic and ultrastructural pathology seen in an explanted heart from a patient with de novo *DES* p. R454W mutation and restrictive cardiomyopathy phenotype. The H&E-stained section shows myocyte hypertrophy and disarray (a, scale bar = 100 µm). Desmin immunohistochemistry demonstrates cytoplasmic aggregates of desmin protein (b, scale bar = 20 µm). Transmission electron microscopy shows electron-dense filamentous material (*) representing desmin aggregates (c, scale bar = 2 µm; d, scale bar = 1 µm).

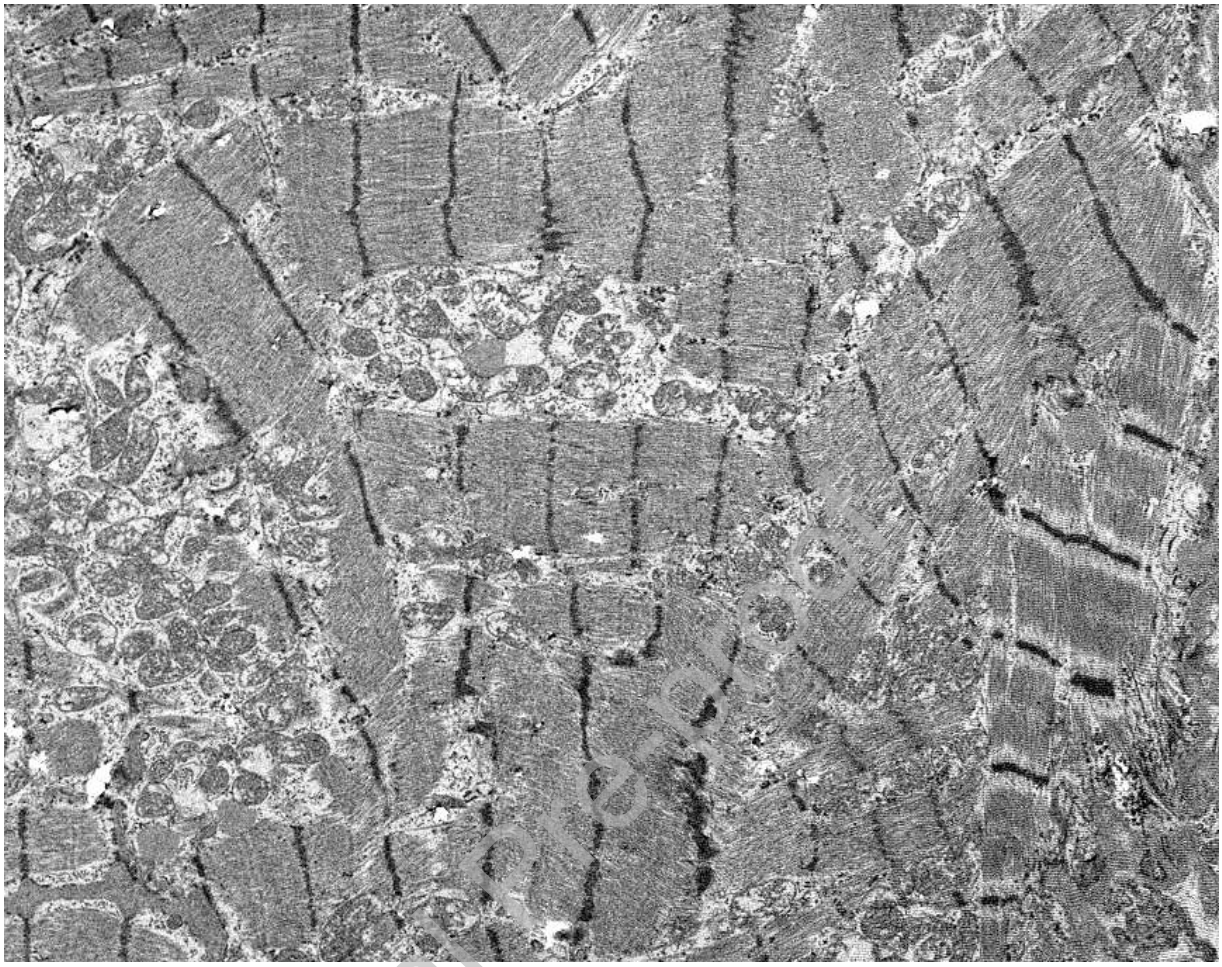

Figure 13. Hypertrophic cardiomyopathy

Myofibrillar disarray in a patient with hypertrophic cardiomyopathy. The myofibrils course in all different directions.

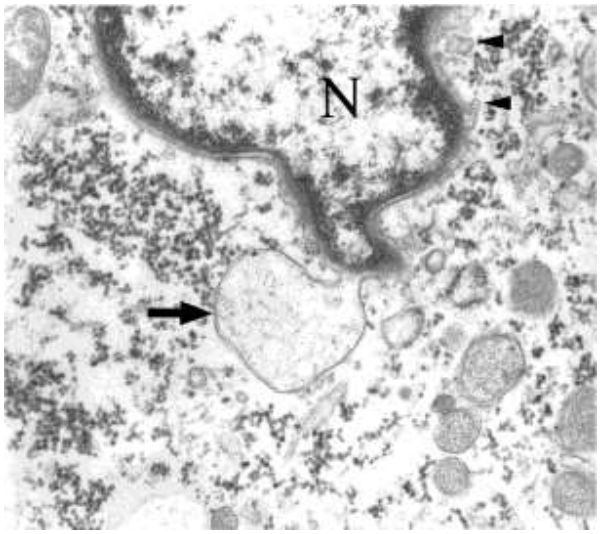

Figure 14. Lamin A/C (LMNA) cardiomyopathy

Disruption of the nuclear lamina resulting in large bleb (arrow) and small bleb (arrowheads) formation (X43000; from *Diercks, et al.* [30] with permission; 10.1016/j.carpath.2009.03.001)

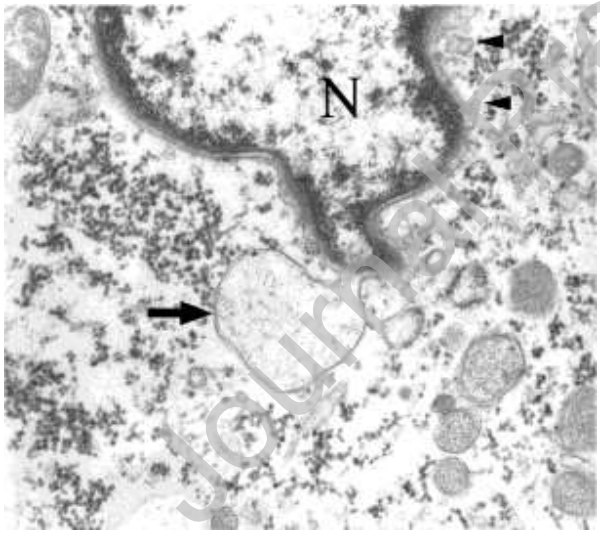

Figure 15. TTN-associated dilated cardiomyopathy

In cases of dilated cardiomyopathy associated with truncating *TTN* mutations, marked nuclear irregularity was observed on H&E-stained slides (inlay) and electron microscopy (X12000; images courtesy of Dr. Richard Mitchell, Harvard University, Boston, MA, USA).

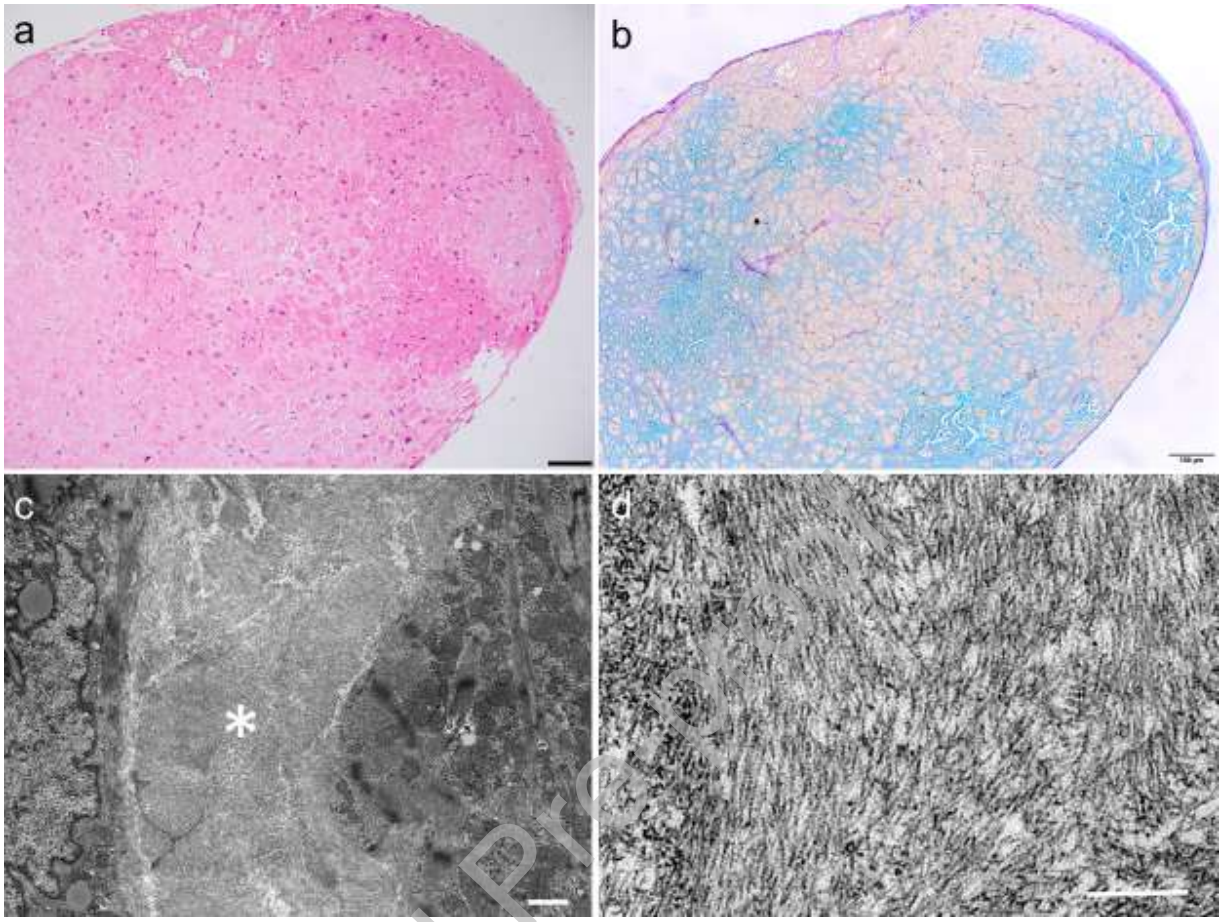

Figure 16. Cardiac amyloidosis

H&E-stained section of heart demonstrating nodular and interstitial deposits of glassy, amorphous eosinophilic material (a, scale bar = 100 µm). The material is seafoam green on the sulfated Alcian blue stain, confirming amyloid (b, scale bar = 100 µm). Ultrastructurally, the material comprises extracellular bundles of non-branching fibrils ranging from 6-13 nm in diameter and 100-1600 nm in length (c, scale bar = 1 µm; d, scale bar = 300 nm).

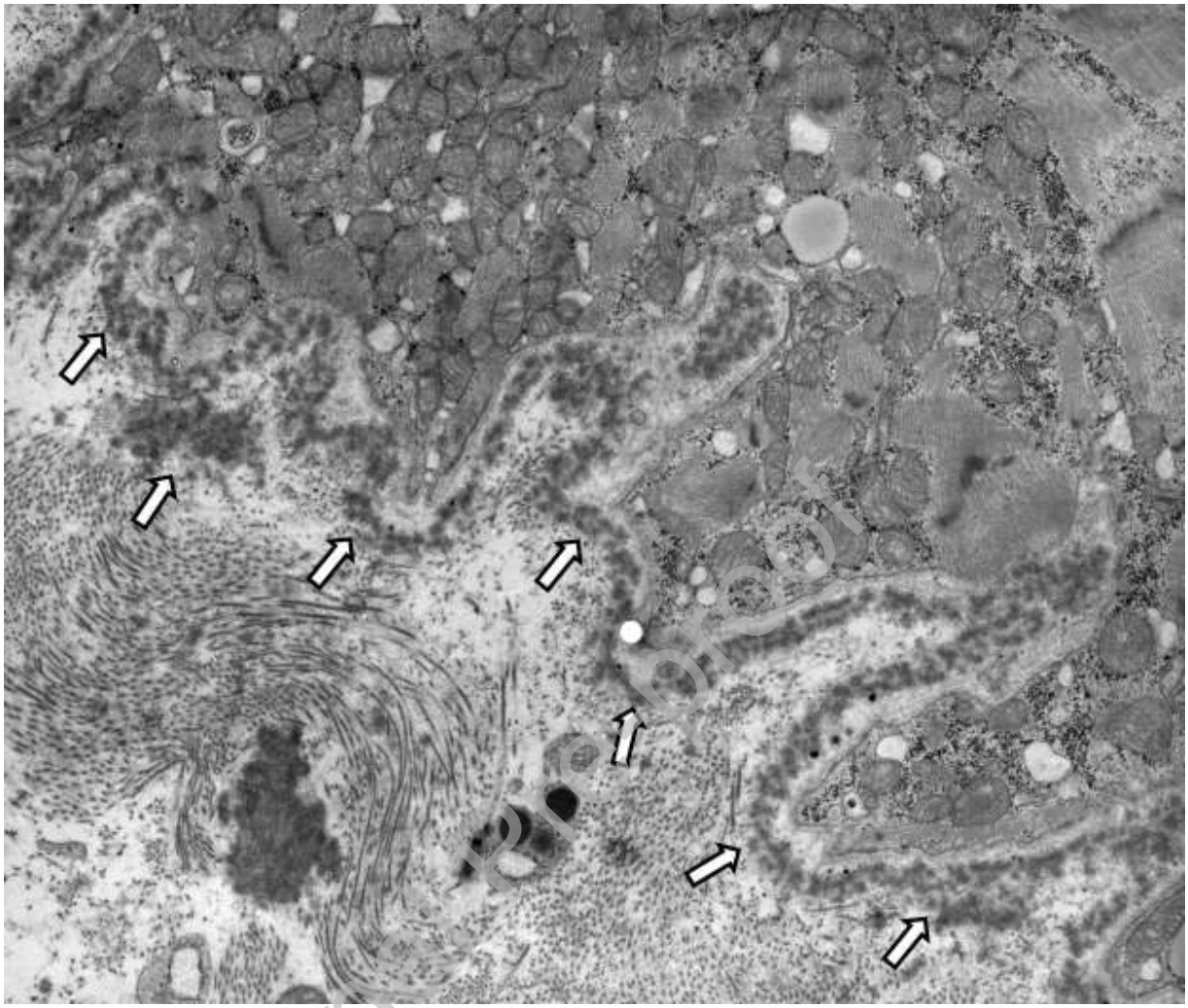

Figure 17. Light chain deposition disease (LCDD)

Powdery, “cotton ball”-like electron dense deposits of light chains (arrows) accumulate along the sarcoplasmic membrane.

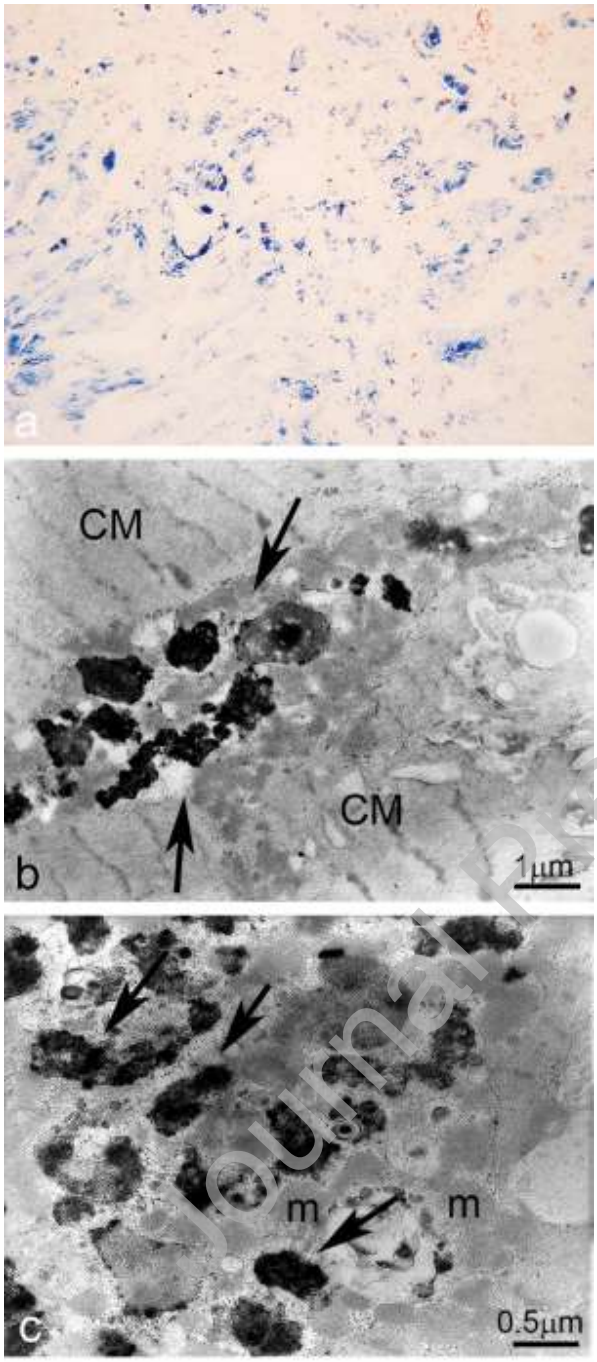

Figure 18. Iron overload

a) Cardiac myocytes show numerous sarcoplasmic granular deposits of hemosiderin (Perls stain, original magnification 5x). b-c) Electron micrograph of cardiomyocytes showing electron-dense lysosomes containing iron deposits (arrows). CM = cardiomyocyte; m = mitochondria

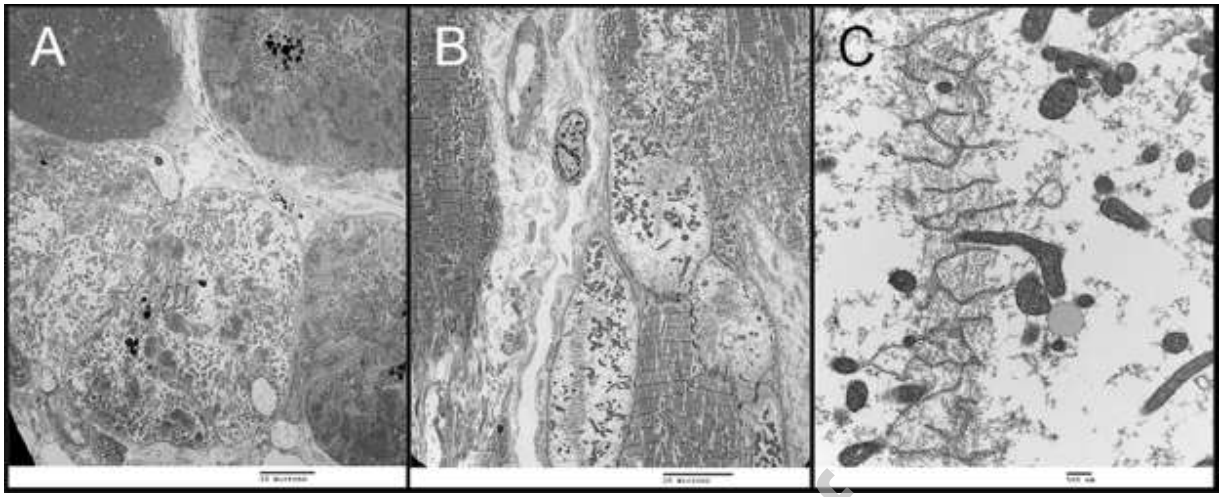

Figure 19. Doxorubicin-induced cardiotoxicity

Ultrastructural changes in doxorubicin-induced cardiotoxicity. Early changes include diffuse sarcolemmic changes within rare cells (A, lower left), compared to unaffected cells nearby. Myofibrillar loss becomes more apparent as the disease progresses (B), while marked changes include organelle degeneration (C).

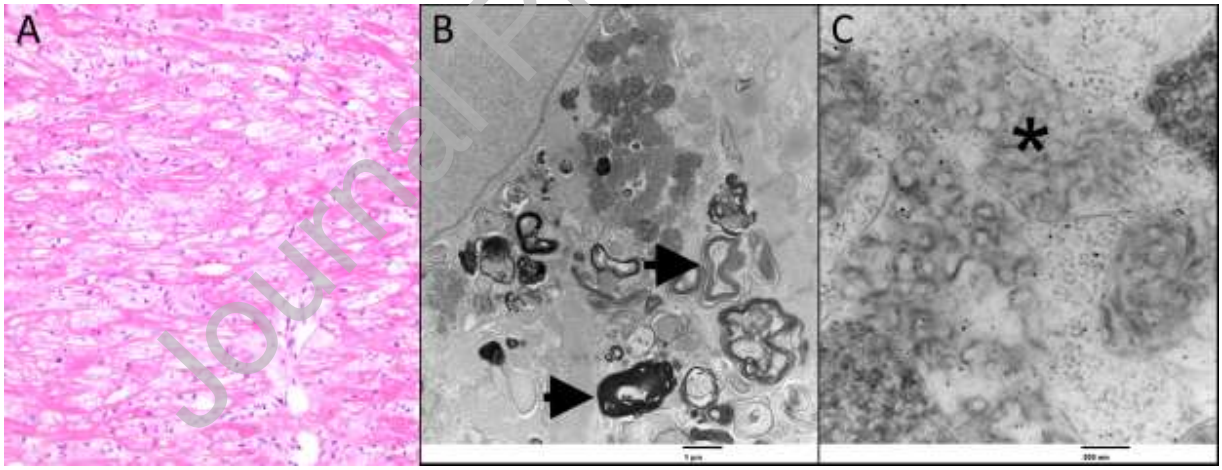

Figure 20. Hydroxychloroquine-induced cardiotoxicity

Hydroxychloroquine-induced cardiotoxicity. Light microscopy shows diffuse sarcolemmic vacuolization (A, hematoxylin and eosin, 100x original magnification). Ultrastructural changes in hydroxychloroquine-induced cardiotoxicity. Owing to lysosomal changes, myelin-like (lamellar) figures are present (B, arrows) along with curvilinear bodies (C, asterisk).

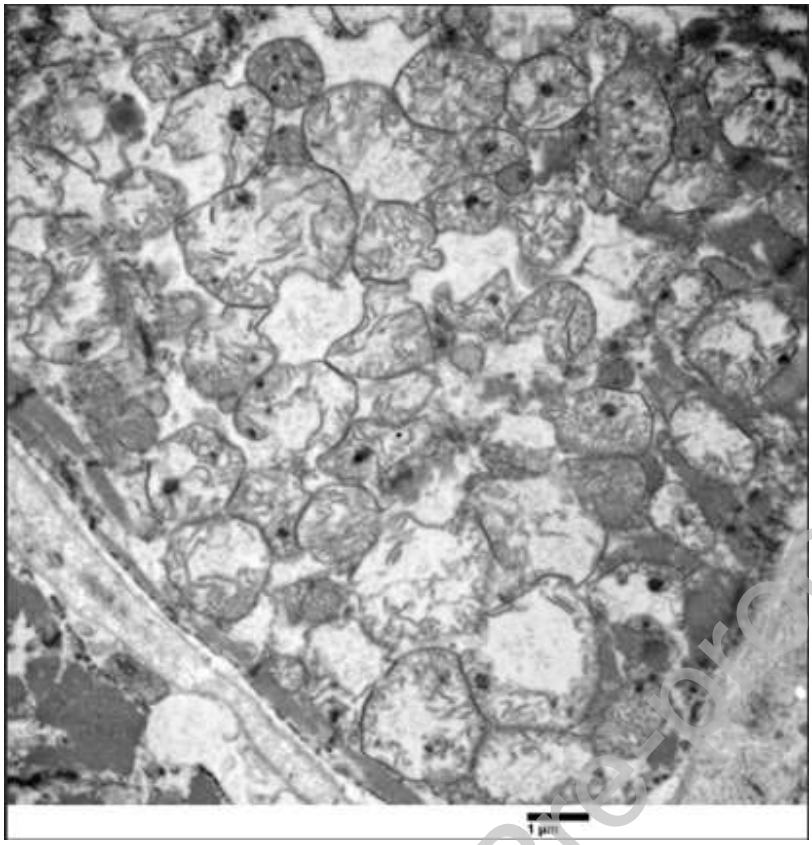

Figure 21. Mitochondrial electron dense bodies

Mitochondrial electron dense bodies. Non-specific densities have been observed in mitochondria in both cardiotoxic conditions and ischemic etiologies, likely representing irreversible organelle damage.

Table 1. Organelles and specialized structures in different types of myocytes

	Atrial Myocytes	Ventricular Myocytes	Purkinje Myocytes
Dimension and Shape	Width: 6 – 8 µm Length: 20 µm Elliptical	Width: 15 – 20 µm Length: 100 µm Cylindrical & branched	Width up to 80µm
Cell contents:			
Myofibrils	Long parallel rows	Long parallel rows	Long parallel rows
Mitochondria	Less abundant than ventricular myocytes	Most abundant	Less abundant than Ventricular myocytes
Glycogen	Between myofibrils and mitochondria	Between myofibrils and mitochondria	Large pools between myofibrils and subsarcolemmal

Granules	Atrial granules (ANF)	Residual bodies	
Transverse tubular system	Absent	Abundant	Absent
Sarcoplasmic reticulum	Abundant	Abundant	Absent
Intercellular Linkages:			
Intercalated discs	Short, predominantly parallel the long axis of myocytes Scant perpendicular discs	Perpendicular to long axis of myocytes, stepwise configuration Scant parallel to the long axis of myocytes	Oblique and zigzag course Greatest surface area of all myocytes
Side-to-side connections	Principal location of cell-to-cell connections	Brief and infrequent	Abundant

Modified from Legato MJ [13] ANF = atrial natriuretic factor

Table 2. Built-in measurements

	Diameter	Length
	nm	**µm**
Sarcomere		2.2
T-Tubules	20 - 450	
Z-band	100 - 140	
I-band		0.7*
A-band		1.5
M-band	25	
Actin	5 – 7	1
Myosin	30	1.6
Intermediate filaments	10	
Microtubules	25	
Ribosomes	20-30	
Mitochondrion		0.5 – 1
Lipid droplets / vacuoles		1
Pinocytic vesicles	100 – 200	
Lysosome		0.2 – 0.3
Lipofuscin		0.5 – 3
Double membrane	4	
Glycogen alpha particles	300	
Glycogen beta particles	20	
Iron particles	0.75 – 1	
Basal lamina	20-50	
Amyloid fibril	10	
Collagen banding	64	

*In relaxed sarcomeres

Table 3. Categories of inborn errors of metabolism

1. Disorders of glycogen metabolism
2. Lysosomal storage diseases
3. Disorders of amino acid metabolism
4. Mitochondrial disorders
5. Peroxisomal disorders

6. Disorders of fatty acid metabolism 7. Cholesterol biosynthesis defects 8. Iron Metabolism Disorders

Table 4. Subtypes of amyloid that affect the heart.

Amyloid subtype	Precursor protein	Etiology
ATTR	Transthyretin	Age-related or hereditary
AL	Immunoglobulin light chain (kappa or lambda)	Plasma cell dyscrasia
AH	Immunoglobulin heavy chain	Plasma cell dyscrasia
AA	Amyloid A protein	Systemic inflammatory disease (e.g. rheumatoid arthritis)
Aβ_2M	β_2-microglobulin	Hemodialysis
AApoAI	Apolipoprotein A-I	Hereditary
AApoAII	Apolipoprotein A-II	Hereditary
AApoAIV	Apolipoprotein A-IV	Unknown
AGel	Gelsolin	Hereditary
ALys	Lysozyme	Hereditary
ALECT2	Leucocyte chemotactic factor 2 (LECT2)	Unknown
AANF	Atrial natriuretic factor (ANF)	Age-related

Table 5. Ultrastructural grading of doxorubicin-induced injury, derived from Billingham et al. [58]

Grade	**Definition**
0	Normal
1	Rare myocytes with early changes*
2	Aggregates of myocytes with definitive changes*
3	Diffuse myocytes with marked changes†

*myofibrillar loss, sarcoplasmic vacuolization
†loss of contractile elements and organelles

Declaration of Competing Interest

The authors declare that they have no known competing financial interests or personal relationships that could have appeared to influence the work reported in this article.